

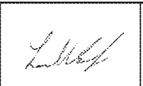
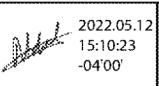


<b>ALSTOM</b> · mobility by nature ·	<b>LRV 1119 Derailment Investigation Report (LeCreusot Technical Team)</b>	Document Reference: <b>DED0002013535</b> Version A	Application date: <b>2022-05-10</b>
<b>Written by:</b>	N. Sembeyev / Transmission Design Engineer C. Benais / Transmission Expert P. Boichot / WCE Master Expert RSC JP. Lefebvre / Design Engineer FEM D. Song / Bogie Project Engineering Manager		
<b>Verified by:</b>	L. VALETTE / Bogie Design Manager	Ensures that the technical/ process accuracy has been checked.	
<b>Approved by:</b>	F. BRUN / Bogie Engineering Warranty Manager	Orders, by his signature, the implementation of the document.	

## COVER PAGE



				2022.05.12 15:10:23 -04'00'	<b>ALSTOM</b>  Alstom Transportation Inc. 805 Belfast Road Ottawa, ON
F. Brun	G. Al Alami	L. Goudge	R. Adnot		
<b>DATE</b>	<b>ESTABLISHED</b>	<b>CHECKED</b>	<b>APPROVED</b>		
<b>DISTRIBUTION</b>	Confidentiality Category Restricted <input type="checkbox"/> Normal <input checked="" type="checkbox"/>	Control Category Controlled <input checked="" type="checkbox"/> Not Controlled <input type="checkbox"/>			
CONFIDENTIAL All rights reserved. ALSTOM	Passing on and copying of this document, use and communication of its content are not permitted without prior written authorization.			<b>DED0002013535</b>	Lang. <b>en</b> N.Shts <b>42</b>

<b>EXECUTIVE SUMMARY.....</b>	<b>6</b>
<b>SECTION 1 SCOPE.....</b>	<b>7</b>
<b>SECTION 2 CONTEXT OVERVIEW.....</b>	<b>7</b>
2.1 Incident overview.....	7
2.2 Design overview .....	8
2.3 Root-cause synthesis.....	10
2.3.1 Analysis.....	10
2.3.2 Focus on root-cause phenomenon .....	11
2.3.3 Fretting phenomenon.....	12
2.4 Investigation roadmap .....	13
<b>SECTION 3 INVESTIGATIONS &amp; PRELIMINARY RESULTS .....</b>	<b>14</b>
3.1 On track test.....	14
3.1.1 Test description.....	14
3.1.2 Test results.....	15
3.1.3 Correlation of Stress with Y-Q calculated from Rwd .....	18
3.1.4 Other observations.....	19
3.1.5 Comparison track quality with 01/2021 test .....	23
3.2 Finite Element Analysis .....	26
3.2.1 Calculation model.....	26
3.2.2 Key parameters & hypotheses .....	30
3.2.3 Calculation results.....	31
3.2.4 Correlation with test results .....	37
3.3 Analytical approach.....	39
<b>SECTION 4 PRELIMINARY CONCLUSIONS &amp; RECOMMENDATIONS .....</b>	<b>40</b>
4.1 Preliminary conclusions & Further investigations .....	40
4.2 Recommendations.....	40
<b>APPENDIX 41</b>	

UNCONTROLLED WHEN PRINTED – Not to be used before verification of applicable version number

**“CONFIDENTIAL - TRADE SECRET” - © ALSTOM SA 2020. All rights reserved. Reproduction, use or disclosure to third parties, without express written authorisation, is strictly prohibited.**

<b>4.3</b>	<b>Appendix 1: Bench test .....</b>	<b>41</b>
<b>SECTION 5</b>	<b>REFERENCES .....</b>	<b>42</b>
<b>SECTION 6</b>	<b>List of Contributors .....</b>	<b>42</b>

*UNCONTROLLED WHEN PRINTED – Not to be used before verification of applicable version number*

***“CONFIDENTIAL - TRADE SECRET” - © ALSTOM SA 2020. All rights reserved. Reproduction, use or disclosure to third parties, without express written authorisation, is strictly prohibited.***

## TABLE OF THE FIGURES

Figure 1 – Map of incident site .....	7
Figure 2 – LRV 19 Axle 2 failure.....	7
Figure 3 – Evidence of slip/slide activity in build up to catastrophic failure.....	8
Figure 4 : Global arrangement of the Ottawa bogie and focus on the axle architecture .....	9
Figure 5 : Cross cut of the axle and focus on the cartridge bearing assembly.....	10
Figure 6 – Fretting corrosion under the small bearing.....	11
Figure 7 - Fretting phenomenon .....	12
Figure 8 : Illustration of the test instrumentation (left) and conditions (right).....	14
Figure 9 - Test Configurations.....	15
Figure 10 - Identified characteristic curves.....	15
Figure 11 - Instrumented hub with R12 and R10.....	16
Figure 12 - Max-min analysis per wheel turn from on track data .....	16
Figure 13 – Cyclic stress level evolution from on track data .....	17
Figure 14 – Results extracted from the statistical analysis .....	18
Figure 15 – Fatigue cases: Comparison of the transversal loads.....	19
Figure 16 - Comparison between B15 and B17 measurement.....	20
Figure 17 On track measurement results in different runs.....	20
Figure 18 - Instrumented bearing spacer .....	22
Figure 19 - Comparison of 2021 VS 2022 Peak acceleration level on axle box.....	23
Figure 20 - Comparison 2021 VS 2022 RMS acceleration level on axle box.....	24
Figure 21 - Comparison 2021 VS 2022 PSD analysis .....	24
Figure 22 - East Bound Track RMS comparison 2021 VS 2022 (results expressed in g) .....	25
Figure 23 - Global overview of the FE model.....	26
Figure 24 - Cut section of the numerical model.....	26
Figure 25 - Contact conditions applied to the interfaces .....	27
Figure 26 – Overview of the boundary conditions .....	28
Figure 27 – Wheel/track load introduction points – Extract from EN 13979-1 .....	28
Figure 28 – Applied loads description on the FEM .....	29
Figure 29 – Workflow for comparing stresses from measurements and calculations.....	30
Figure 30 – Curve load case – Evolution of the contact pressure depending on curve loads .....	31
Figure 31 – Curve load case – Evolution of the contact gap depending on curve loads.....	32

UNCONTROLLED WHEN PRINTED – Not to be used before verification of applicable version number

**“CONFIDENTIAL - TRADE SECRET” - © ALSTOM SA 2020. All rights reserved. Reproduction, use or disclosure to third parties, without express written authorisation, is strictly prohibited.**



Figure 32 – Curve load case – Visualisation of the deformed shape under the small bearing .....	33
Figure 33 – Curve load case – Analysis of the areas of contact loss .....	33
Figure 34 – Gearbox Inertia – Variation of the contact pressure – Comparison with Curves cases .....	34
Figure 35 – Comparison of the variation of contact pressure for Curves and Gearbox Inertia .....	34
Figure 36 – Gearbox Inertia – Evolution of the contact gap – Comparison with Curves cases .....	35
Figure 37 – Gearbox Inertia – Analysis of the areas of contact loss .....	35
Figure 38 – Measurements / Calculations – Stresses for R12 & Rlt0 locations for Curves 3 & 5 .....	37
Figure 39 – Measurements / Calculations – Link between the stresses in R12 and Rlt0 .....	38

*UNCONTROLLED WHEN PRINTED – Not to be used before verification of applicable version number*

***“CONFIDENTIAL - TRADE SECRET” - © ALSTOM SA 2020. All rights reserved. Reproduction, use or disclosure to third parties, without express written authorisation, is strictly prohibited.***

## EXECUTIVE SUMMARY

This report is preliminary in nature and further investigations will be required to decisively conclude on the exact root cause of the issue.

The root-cause analysis demonstrates that the actual design of the track generates excessive transversal loads/forces that causes excessive fretting under the bearing of the axle. This fretting could lead to a contact wear, that will generate axial clearance within the bearing assembly. The axial clearance is occurring on the Ottawa fleet at an accelerated and unprecedented rate with severe consequences not experienced on any other ALSTOM product operating with the same concept elsewhere in the world.

Based on the analysis, the test and simulations demonstrate that the transversal quasi-static loads mainly generated during curving is a critical factor causing the fretting under the bearing of the axle. These loads are higher on the 2 motor bogies at the extremities of the trainset, mainly due to the exceptionally severe lateral forces on the extreme axles during operation and higher nominal axle load. This is in line with the fleet control status showing a higher percentage of failed axles on leading and trailing bogies at the extremities of the trainset.

On track test results measured in January and February of 2022 that occurred after the track regrounding performed by the maintainer in July of 2021 showed an improvement of track conditions in terms of vibration level (mainly related to rail corrugation in curves) as compared to the January 2021 results, at which point the track was generating a high level of vibration on the bogie. It is logical to consider that these levels of vibration contribute to the increased loads on the assembly during this period of time. Some of the axles being recently detected with a clearance could have been affected by fretting initiated prior to the track regrounding that occurred in June 2021. In summary, at this juncture we can state that the state and configuration of the track is a critical factor leading to the aforementioned fretting phenomenon. It must be stated that the actual as-built track was not in line with the design as stated in the wheel/rail interface specification agreed by OLRTC.

There are several actions that can help correct the situation. These are split into short term and long term as follows:

### Short Term

- Reduction of rail corrugation through maintenance
- Increase track greasing
- Adjustment of speed profile, particularly along curves
- Modify wheel profile to better sustain severe transversal forces exhibited by the track

Upon implementation of some/all of the above points, a review of the 7500km inspection interval can be done in order to reduce the frequency and the associated operational inefficiencies

### Long Term

- Additional track reprofiling, following the improvements seen due to the rework in 2021
- Enhancement of the axle design to withstand transversal loads exhibited by the track

Further investigations need to be conducted in order to evaluate the benefits of each of these points..

*UNCONTROLLED WHEN PRINTED – Not to be used before verification of applicable version number*

***“CONFIDENTIAL - TRADE SECRET” - © ALSTOM SA 2020. All rights reserved. Reproduction, use or disclosure to third parties, without express written authorisation, is strictly prohibited.***

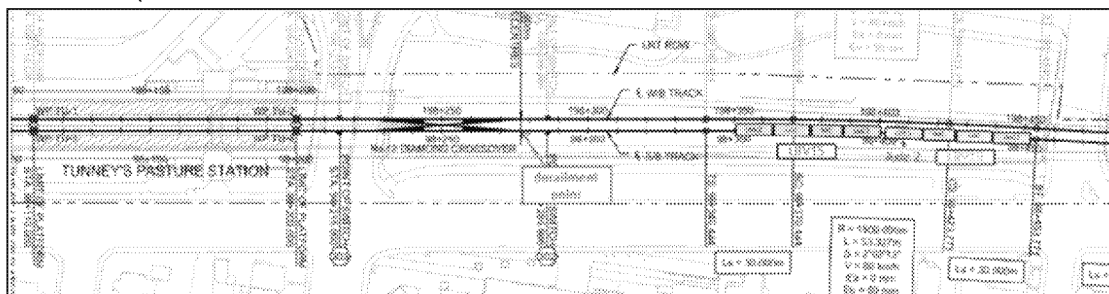
## SECTION 1 SCOPE

The purpose of this report is to document the investigation related to the axial clearance generation in the axle hub cartridge bearing assembly that was identified in the preliminary report on the TS19 derailment. This report presents the global context of the root-cause analysis, preliminary investigations, further analysis to be carried out and recommendations based on current analysis.

## SECTION 2 CONTEXT OVERVIEW

### 2.1 Incident overview

On August 8, 2021 at 20:16 hours, the train was leaving Tunney's Pasture station with LRV15 and LRV19 coupled together and LRV19 LMC2 leading when the axle hub (gearbox side) of axle 2 failed and the wheel assembly separated from the axle leading to the derailment of this axle. The derailment occurred on the straight portion of Track 2 with no superelevation immediately after the passage of the #12 crossover (Switch 302) – see Figure 1 below. Prior to departure the coupled train was stabled on Track 1 at the station platform for around 5 hours.



**Figure 1 – Map of incident site**

On site examination of the failed axle assembly shows that significant heat and abrasion of the mechanical parts led to failure. See Figure 2 below.



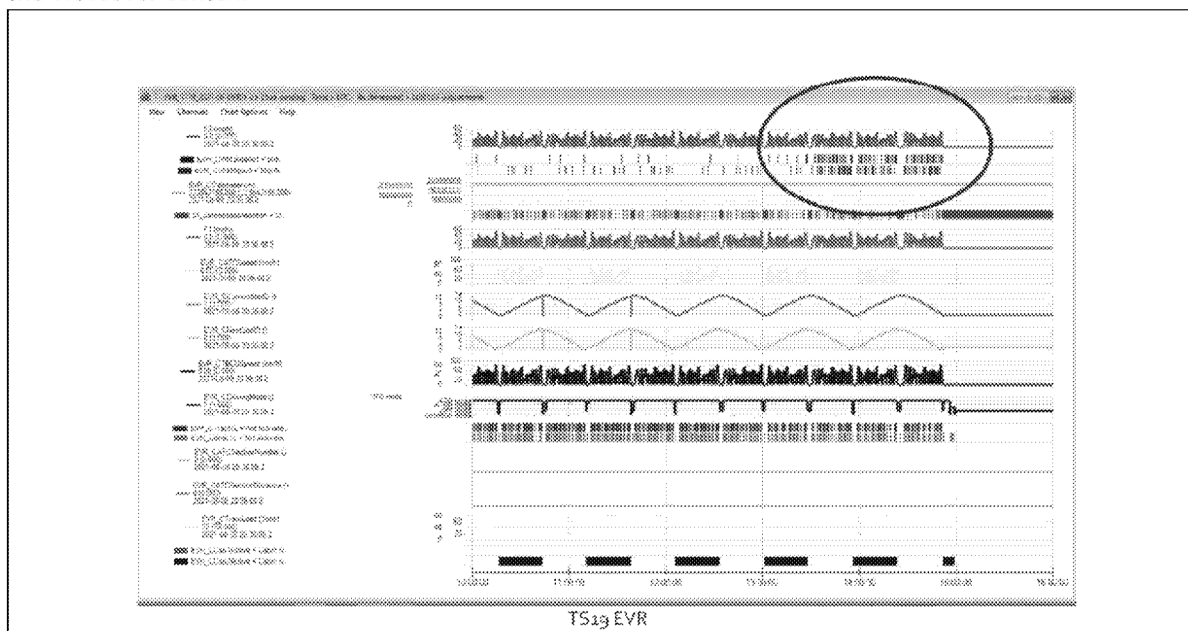
**Figure 2 – LRV 19 Axle 2 failure**

UNCONTROLLED WHEN PRINTED – Not to be used before verification of applicable version number

**“CONFIDENTIAL - TRADE SECRET” - © ALSTOM SA 2020. All rights reserved. Reproduction, use or disclosure to third parties, without express written authorisation, is strictly prohibited.**



Analysis of the LRV data leading up to the failure shows that axle 2 had been showing significant slip/slide events in the preceding 90 minutes (see Figure 3 below). This is indicative of a loss of integrity of the splined axle connection between the two wheels as the failure of the cartridge and bearing mechanism progressed to a critical point. This data was taken from the operational period immediately preceding the LRV being stabled at Tunney's Pasture at 3pm on 8th August. At this point, it is thought that the failed drive cooled, seized, and upon subsequent departure from Tunney's Pasture at 8pm failed as it transited the crossover switch.



**Figure 3 – Evidence of slip/slide activity in build up to catastrophic failure**

## 2.2 Design overview

Each bogie of the Ottawa trainset is equipped with the same 2 axles being differently equipped depending on their position on the train.

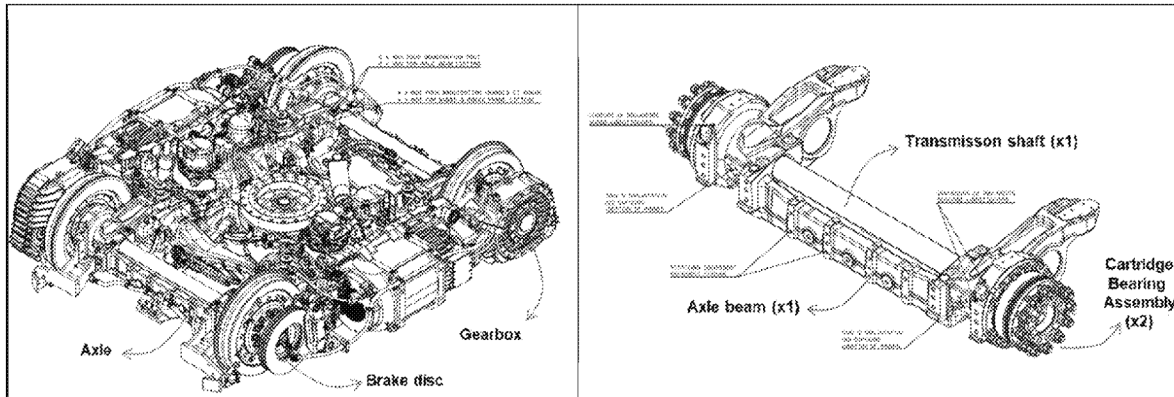
Each axle is composed of 1x Axle beam, 1x Transmission shaft and 2x Cartridge Bearing Assembly (CBA).

The Cartridge Bearing Assembly (CBA) is a sub assembly of the axle which is connected to the axle beam on one side. On the other side of the CBA is attached the wheel as well as a gearbox or a brake disc depending on the position of the axle on the bogies.

UNCONTROLLED WHEN PRINTED – Not to be used before verification of applicable version number

**“CONFIDENTIAL - TRADE SECRET” - © ALSTOM SA 2020. All rights reserved. Reproduction, use or disclosure to third parties, without express written authorisation, is strictly prohibited.**





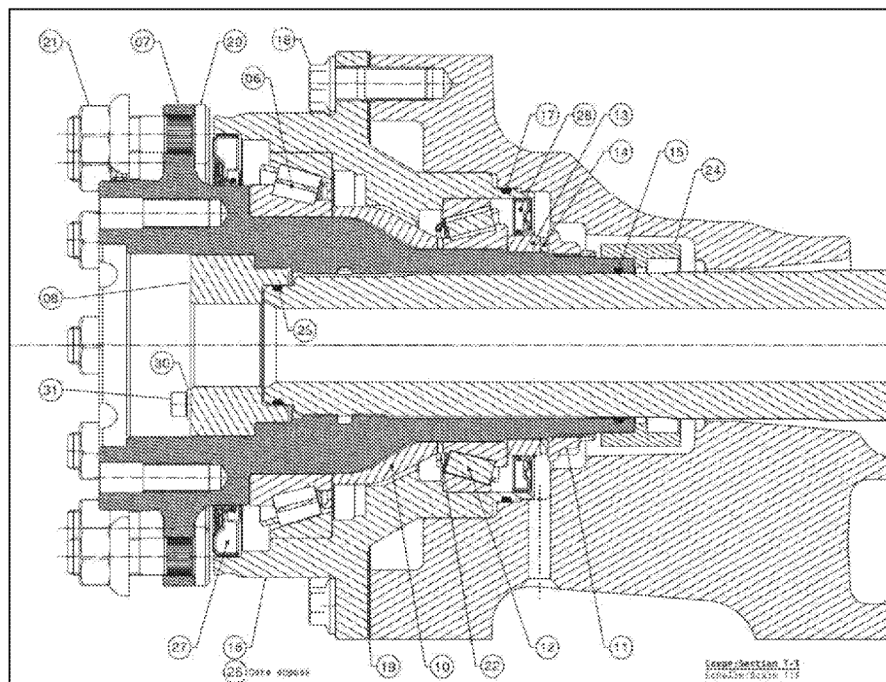
**Figure 4 : Global arrangement of the Ottawa bogie and focus on the axle architecture**

The CBA is mainly constituted of:

- 1x Bearing sleeve (#16 or #26 depending on the side) which allows the assembly to be fixed on the axle beam and where the outer ring of the bearings is fitted. This part is static during operation.
- 1x Hub (#07) where the wheel is mounted (with the studs #20 and nut #21). This part is rotating during operation and transfers different kinds of loads (for better understanding see Figure 29, §3.2.1)
  - o The traction/braking loads coming from the gearbox/disc attached at the extremity of the hub, or the spline of the shaft which goes through the hub
  - o The static and dynamic load coming from the wheel related to :
    - The vertical (Q) and lateral quasi-static loads (Y) induced by the weight of the car body and the bogie
    - The vertical (dQ) and lateral (dY) dynamic loads induced by the dynamic of the vehicle during operation
  - o The static and dynamic loads coming from the moment of inertia of the components (gearbox or disc) attached to the axle
- 2x Bearings which allow the rotation of the hub into the sleeve. The bearing arrangement is set with:
  - o 2 conical bearings which are assembled to achieve a "no preload/no clearance" setting (bearing #06 being called for simplification purpose "Big bearing", whereas the bearing #12 will be called "Small bearing"). The bearings are grease lubricated.
  - o A spacer (#10) which separates both bearings inner rings
  - o A setting shim (#22) which allows to achieve the clearance setting
  - o A locking nut (#11) that closes the stack of the bearing assembly on the hub (the nut is tightened and crimped on the hub)
- Other components of the assembly insure the grease tightness (dynamic seals (#27/28), o'rings (#17/15)). The part #08 relative to current return is not at stake in this problematic as well as the phonic wheel #24 which is used for speed control.

UNCONTROLLED WHEN PRINTED – Not to be used before verification of applicable version number

**"CONFIDENTIAL - TRADE SECRET"** - © ALSTOM SA 2020. All rights reserved. Reproduction, use or disclosure to third parties, without express written authorisation, is strictly prohibited.



**Figure 5 : Cross cut of the axle and focus on the cartridge bearing assembly**

## 2.3 Root-cause synthesis

### 2.3.1 Analysis

The analysis of all available information suggests the following sequence of events

- increase of cartridge bearing assembly (CBA) axial clearance,
- subsequent loss of bearings pre-load,
- misalignment, unexpected contacts, eventual thermal runaway and
- subsequent bearings failure.

The root-cause analysis utilizing ISHIKAWA methodology investigated possible causes of CBA axial clearance increase that initiates the failure mechanism of the assembly.

The manufacturing process of Texelis was analyzed including among other things the check of the torque tightening of the assembly and the axial clearance setting process. The results of the verifications allowed to exclude the manufacturing process and a human factor from the root-cause of axial clearance.

Further development of the investigation revealed the phenomenon of excessive fretting under the inner ring of the small bearing fitted on the hub to be at the origin of CBA axial clearance increase.

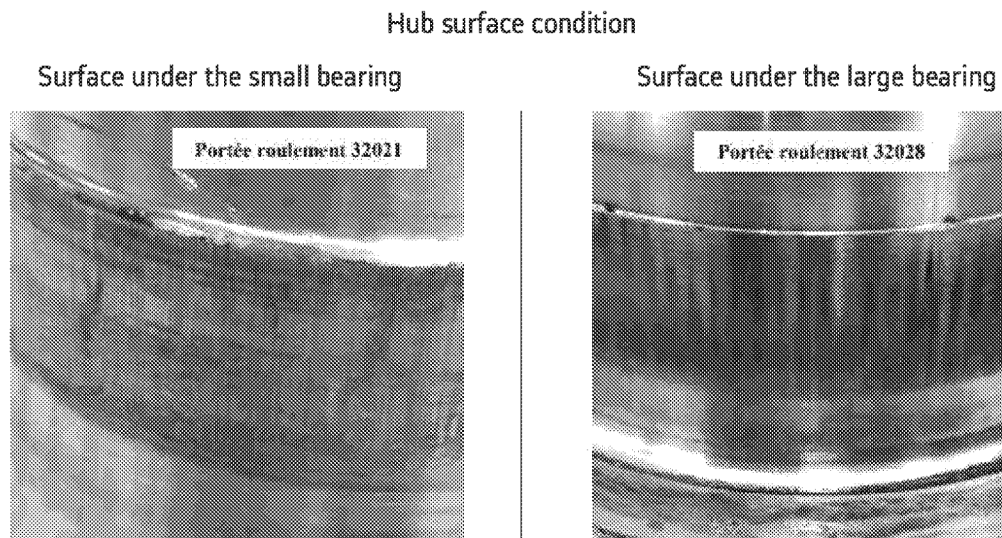
*UNCONTROLLED WHEN PRINTED – Not to be used before verification of applicable version number*

**“CONFIDENTIAL - TRADE SECRET” - © ALSTOM SA 2020. All rights reserved. Reproduction, use or disclosure to third parties, without express written authorisation, is strictly prohibited.**



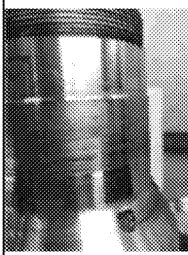

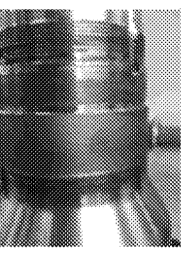
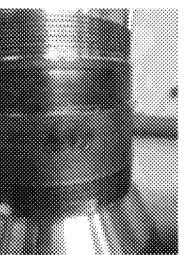
### 2.3.2 Focus on root-cause phenomenon

During the technical evaluation of the parts, the fretting phenomenon was observed on the surface of the hub (part #7, Figure 6) under the small bearing (part #12) while no fretting was present under the large bearing (part #6).



**Figure 6 – Fretting corrosion under the small bearing**

The comparative observations of the hubs showed that higher values of fretting wear under small bearing corresponded to higher values of axial clearance of respective CBA as can be seen in the table below.

Hub s/n	195249	195251	190366	186839
Axial clearance, mm	0,03	0,06	0,320	0,571
Hub photo				
Comments	Almost complete loss of bearing preload	Complete loss of bearing preload Scratch evidence	Complete loss of bearing preload and nut torque	Complete loss of bearing preload and nut torque

**Table 1. Hub fretting condition as a function of CBA axial clearance**

UNCONTROLLED WHEN PRINTED – Not to be used before verification of applicable version number

“CONFIDENTIAL - TRADE SECRET” - © ALSTOM SA 2020. All rights reserved. Reproduction, use or disclosure to third parties, without express written authorisation, is strictly prohibited.

When the fretting under the small bearing becomes excessive, it leads to a contact wear that can generate a loss of fit under the bearing, as well as axial clearance on the bearing seat. This consequently, or in parallel, will lead to another fretting phenomenon within the stack that finally generates the observed bearing clearance.

Additionally, it is to be noted, that the frequency of increased axial clearance by location along the trainset (developed through the ongoing monitoring program) demonstrates that a significant proportion of all CBAs that exhibited increasing axial clearance, are at the extremities of the trainset (83%).

BM1		BP1				BM2				BP2				BM3					
Axle 1		Axle 2		Axle 3		Axle 4		Axle 5		Axle 6		Axle 7		Axle 8		Axle 11		Axle 12	
Left	Right	Left	Right	Left	Right	Left	Right	Left	Right	Left	Right	Left	Right	Left	Right	Left	Right	Left	Right
4	5	9	5	0	1	1	0	3	0	1	0	0	2	0	0	4	4	6	4

**Figure 7 : Distribution of Axle play out of Limits (BM1 & BM3 are the bogie at the extremities)**

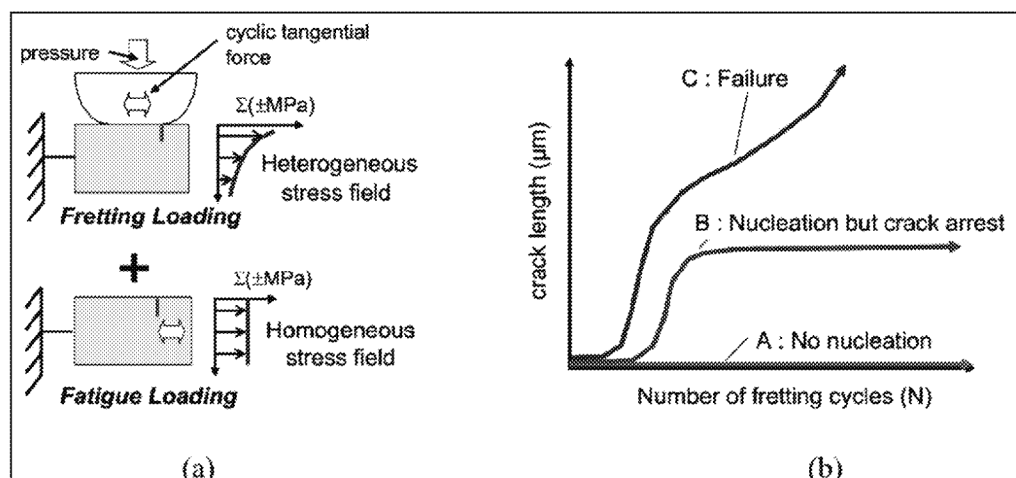
### 2.3.3 Fretting phenomenon

Fretting is a very common phenomenon on the seat and the bore of a bearing assembly. 3 main parameters can lead to it:

- Micro displacement between 2 fitted parts (usually in the range of 0.01 to 0.1mm)
- Contact pressure between the 2 fitted parts
- Friction coefficient between these 2 fitted parts.

These 3 parameters cause a surface stress which can generate:

- Dark area which is acceptable and without risk for the parts (Minor fretting)
- Red powder (Fretting corrosion) which is more severe and can cause wear and failure
- Crack nucleation which generates surface degradation and wear
- Crack propagation which are critical and cause failure.



**Figure 8 - Fretting phenomenon**

UNCONTROLLED WHEN PRINTED – Not to be used before verification of applicable version number

**"CONFIDENTIAL - TRADE SECRET"** - © ALSTOM SA 2020. All rights reserved. Reproduction, use or disclosure to third parties, without express written authorisation, is strictly prohibited.



The previous figure (Figure 8, a) shows the composition of cyclic tangential surface stress due to contact pressure and micro displacement, with the fatigue stress due to shaft flexion.

What we observe after the technical evaluation of the parts is the situation "B" (Figure 8,b). The consequence is a significant wear with a modification of the contacts, the load distribution, etc.

The fretting phenomenon can be the result of different factors in design and/or service conditions. Therefore, the bearing hub assembly is sensitive to several key parameters, as identified below:

- Radial load on the bearing: related to external loads applied to the assembly (Y&Q, gearbox inertia, etc.)
- Geometry of the hub (inertia and diameter)
- Micro-displacement in the transversal and tangential direction: related to the part geometry, bearing fitting parameters, and external loads
- The contact pressure between bearing and shaft: related to the part geometry, bearing fitting parameters, and external loads
- The mechanical characteristics of material
- The friction factor between parts in contact

## 2.4 Investigation roadmap

The investigation approach consisted in using a complex model of CBA using finite-element method with a high level of detail in order to simulate the real behavior of the assembly. A first Model simulation permitted to highlight the areas of interest which are the most sensible to track inputs.

In order to accurately set the Model according to its real behavior, real stress data were collected during an on-track test campaign on Ottawa rail network. The sensors and strain gauges were installed in the areas of interest. The data received from the field was then post-treated, analyzed and the resulted information was used to refine and validate the numerical model.

Eventually, the correlation of track data to the Finite Element Model must enable us to:

- extrapolate the quasistatic loads coming from the operating condition and compare it with the design loads
- refine the analysis of the effect of these loads around the small bearing fit onto the hub

## SECTION 3 INVESTIGATIONS & PRELIMINARY RESULTS

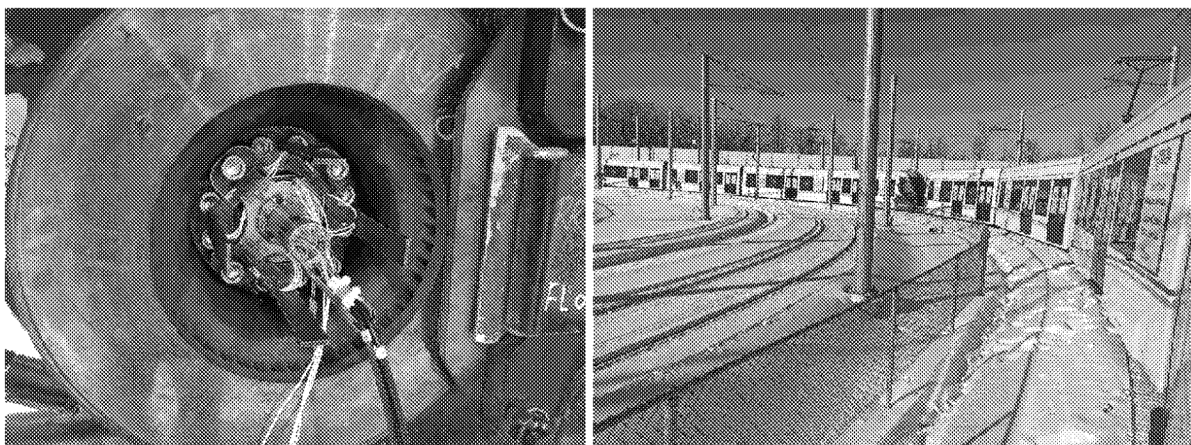
### 3.1 On track test

To evaluate more accurately the loads and mechanism at stake in the assembly during operations, specific testing axles were designed. A full on-track test program (See document [P1] for test plan) was also set to explore the exact impact of different running conditions within the CBA.

In total, 2 months of design and production were needed to prepare the testing axle, with a 2-week final assembly and preparation to ensure the integrity and functionality of the gauges before shipping the axle.

2 sets of telemetry were also adapted and installed on the bogie as well as slip rings. Totally more than 30 measurements were set on the rotating parts to collect the data in live during operation.

In total, 150 channels were instrumented and recorded during the test (stress, speed, accelerations, displacement...). The test campaign was totally performed on 2 weeks (preparation, test runs, uninstallation) with no stops and night and/or days shifts.



**Figure 9 : Illustration of the test instrumentation (left) and conditions (right)**

After the test, 200 hours of post-processing have been already required to analyze and sort the useful or relevant information acquired during the on-track test.

#### 3.1.1 Test description

The on-track test was carried out with Multiple Unit (MU) LRV 15/37. The extremity bogie BM3 on MU was instrumented on both axles. A round way trip was done in all test configurations to gather measurements for both instrumented axles as leading and rear axle as detailed on Figure 10.

*UNCONTROLLED WHEN PRINTED – Not to be used before verification of applicable version number*

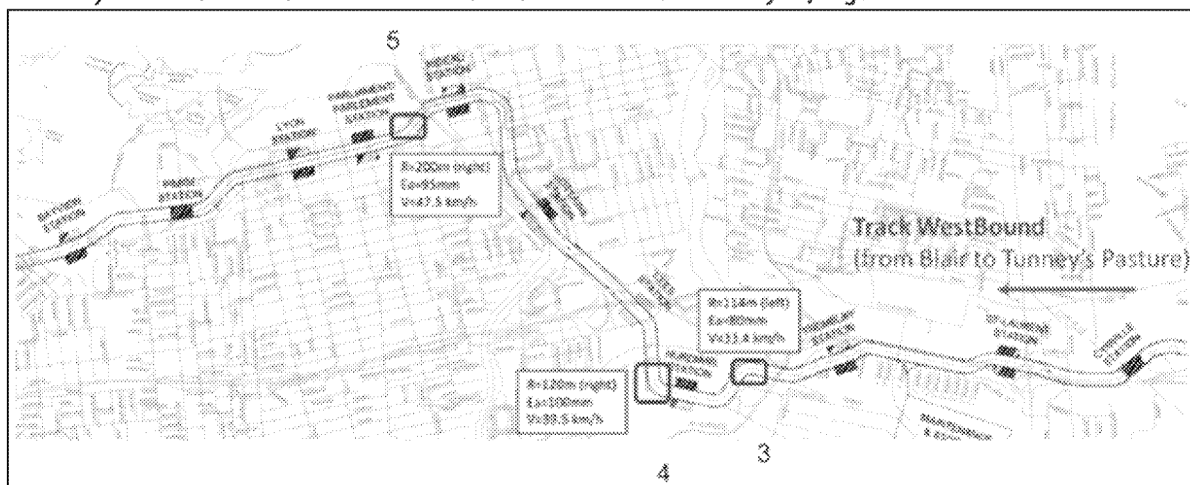
**“CONFIDENTIAL - TRADE SECRET” - © ALSTOM SA 2020. All rights reserved. Reproduction, use or disclosure to third parties, without express written authorisation, is strictly prohibited.**



AW0-B15worn(2000km)			
<2022-01-29 06:07-06 (AW0_B15w_ATO_MC2_WestB_26)>	MC2	Blair	Tunney's WestB
<2022-01-29 07:28-46 (AW0_B15w_ATO_MC1_EastB_29)>	MC1	Tunney's	Blair EastB
AW0-B15worn(2000km)			
<2022-01-29 18:03-21 (AW0_B15w_MC1_WestB_43)>	MC1	Blair	Tunney's WestB
<2022-01-29 18:31-03 (AW0_B15w_MC2_EastB_44)>	MC2	Tunney's	Blair EastB
AW0-S reprof			
<2022-01-31 00:32-57 (AW0_B15n_ATO_MC1_WestB_53)>	MC1	Blair	Tunney's WestB
<2022-01-31 01:00-24 (AW0_B15n_ATO_MC2_EastB_54)>	MC2	Tunney's	Blair EastB
<2022-01-31 03:35-31 (AW0_B15n_ATO_MC2_WestB_61)>	MC2	Blair	Tunney's WestB
<2022-01-31 04:02-31 (AW0_B15n_ATO_MC1_EastB_52)>	MC1	Tunney's	Blair EastB
AW3-B15reprof			
<2022-02-02 01:20-00 (AW3_B15n_ATO_MC2_EastB_77)>	MC2	Tunney's	Blair EastB
<2022-02-02 01:51-34 (AW3_B15n_ATO_MC1_WestB_78)>	MC1	Blair	Tunney's WestB
<2022-02-02 05:09-18 (AW3_B15n_ATO_MC2_WestB_86)>	MC2	Blair	Tunney's WestB
<2022-02-02 05:39-51 (AW3_B15n_ATO_MC1_EastB_87)>	MC1	Tunney's	Blair EastB
AW0-B17			
<2022-02-05 04:24-06 (AW0_B17n_ATO_MC2_EastB_109)>	MC2	Tunney's	Blair EastB
<2022-02-05 04:51-19 (AW0_B17n_ATPM_MC1_WestB_110)>	MC1	Blair	Tunney's WestB
<2022-02-05 06:28-57 (AW0_B17n_ATO_MC2_WestB_114)>	MC2	Blair	Tunney's WestB
<2022-02-05 06:57-36 (AW0_B17n_ATO_MC1_EastB_115)>	MC1	Tunney's	Blair EastB
AW0-B17flat			
<2022-02-06 00:31-38 (AW0_B17flat_ATO_MC2_WestB_124)>	MC2	Blair	Tunney's WestB
<2022-02-06 01:04-51 (AW0_B17flat_ATO_MC1_EastB_125)>	MC1	Tunney's	Blair EastB
<2022-02-06 03:34-09 (AW0_B17flat_ATO_MC1_WestB_129)>	MC1	Blair	Tunney's WestB
<2022-02-06 04:04-16 (AW0_B17flat_ATO_MC2_EastB_130)>	MC2	Tunney's	Blair EastB

**Figure 10 - Test Configurations**

After the first post-processing, the following curves (Curves 3, 4, 5 respectively as WB240, WB220 and WB110) were later identified as "characteristic" for a focused analysis, Figure 11.


**Figure 11 - Identified characteristic curves**

### 3.1.2 Test results

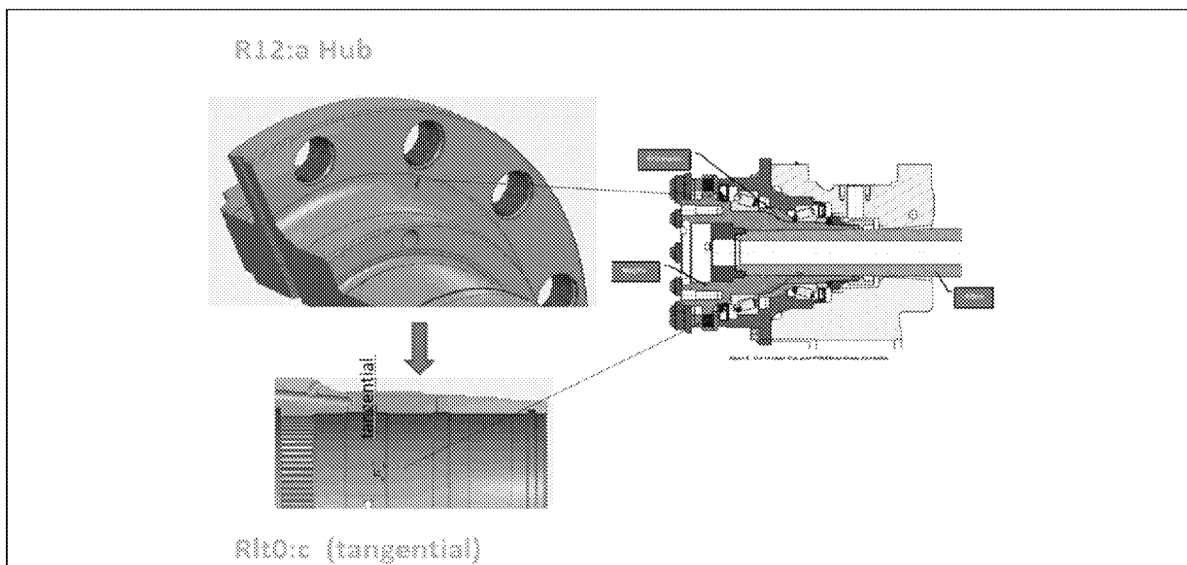
The instrumented axle hub was equipped with strain gauges in Radius 12 (transition area from wheel-hub fixing crown, "R12"). These strain gauges are directly sensitive to transversal Y and vertical Q loads transmitted by wheel/rail contact and are also impacted by vibration & track excitations.

The stress level in R12 during on track measurement was recorded continuously and identified as "R12:a" signal in the following analysis.

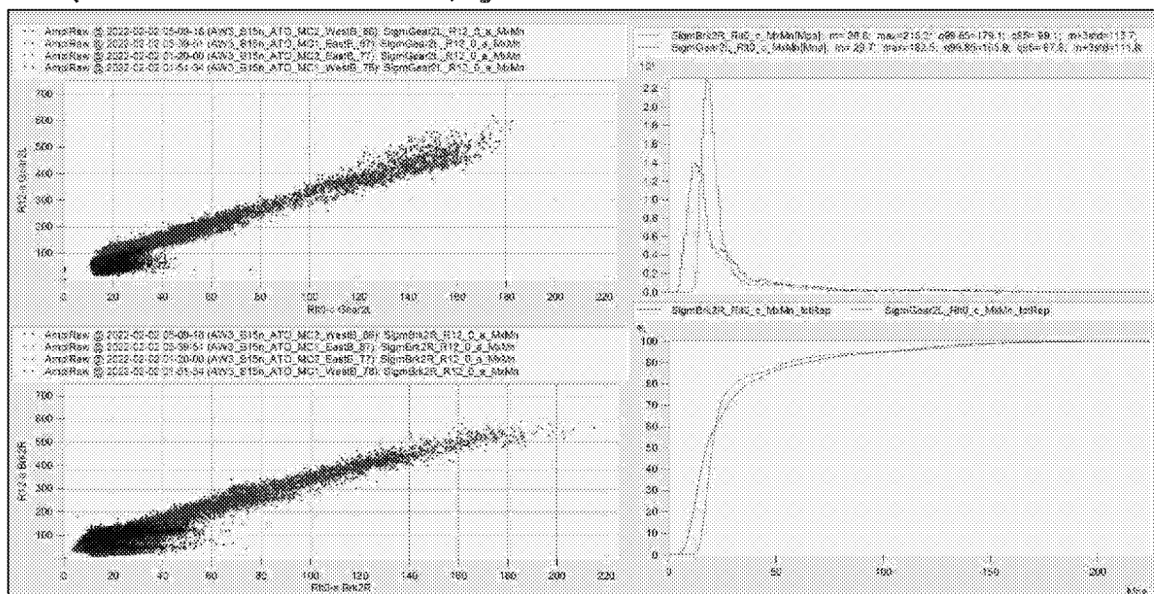
Tri-directional rosettes were located on the section under the small bearing seat area ("R1to").

UNCONTROLLED WHEN PRINTED – Not to be used before verification of applicable version number

**"CONFIDENTIAL - TRADE SECRET"** - © ALSTOM SA 2020. All rights reserved. Reproduction, use or disclosure to third parties, without express written authorisation, is strictly prohibited.


**Figure 12 - Instrumented hub with R12 and RltO**

The tangential stress record identified as "RltO:c" is directly correlated to "R12:a" input, and also sensitive to Y & Q efforts and vibration excitations, Figure 13.


**Figure 13 - Max-min analysis per wheel turn from on track data**

The correlation between "R12:a" and "RltO:c" is shown by Max-Min analysis per wheel turn, at Figure 13. The graphics showed a 0.3 ratio between "RltO:c Mx-Mn" and "R12:a Mx-mn".

During the 2022 test campaign, both areas are mainly sensitive to curving due to the increase of the lateral track forces (Transversal loads > Y effort).

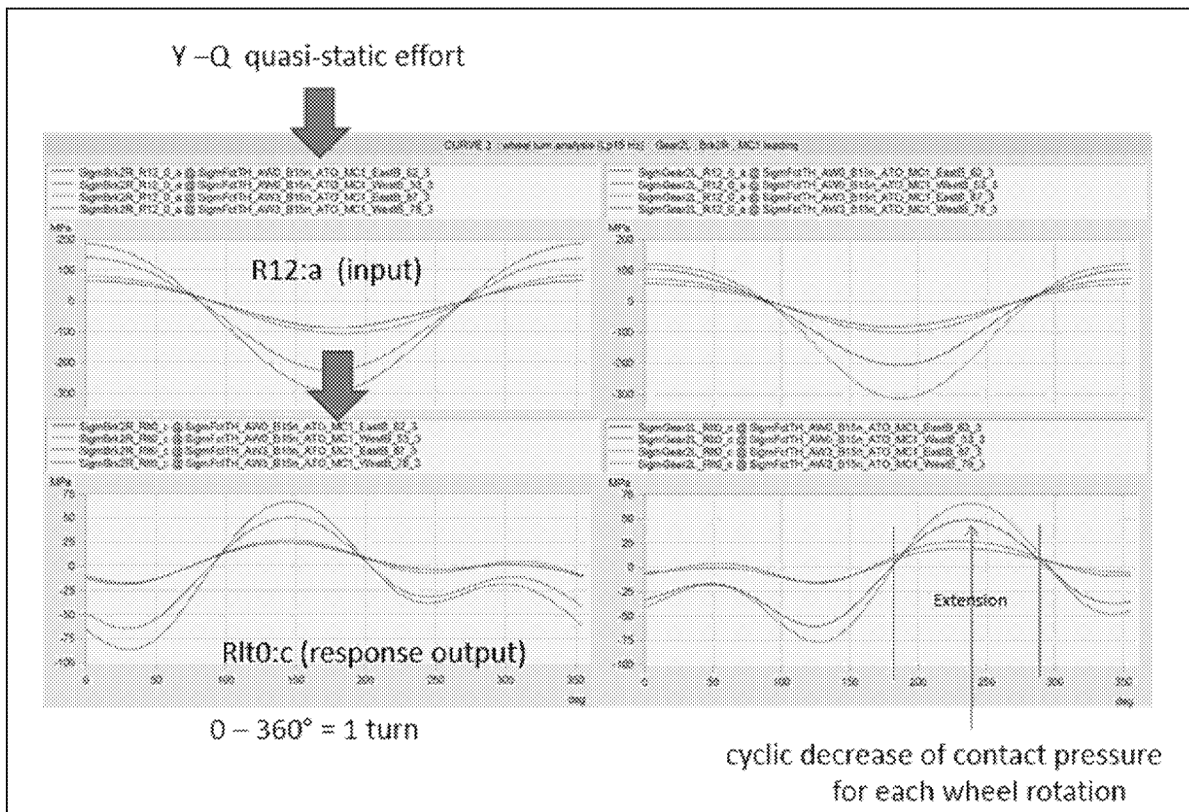
The graphics here after (Figure 14) showed the cyclic evolution for each wheel revolution (0 – 360°). The "R12:a" stress measurement is sensitive to Y – Q quasi-static effort, which conducts then to the "RltO:c" response as an output.

UNCONTROLLED WHEN PRINTED – Not to be used before verification of applicable version number

**"CONFIDENTIAL - TRADE SECRET" - © ALSTOM SA 2020. All rights reserved. Reproduction, use or disclosure to third parties, without express written authorisation, is strictly prohibited.**



The evolution of "Rlt0:c" stress during wheel rotation confirms a cyclic reduction of the contact pressure under the small bearing, that can lead to fretting phenomenon and waving movement of the bearing. This was already a specific behavior detected in the raw finite element analysis performed prior to the test.



**Figure 14 – Cyclic stress level evolution from on track data**

UNCONTROLLED WHEN PRINTED – Not to be used before verification of applicable version number

**"CONFIDENTIAL -TRADE SECRET"** - © ALSTOM SA 2020. All rights reserved. Reproduction, use or disclosure to third parties, without express written authorisation, is strictly prohibited.

### 3.1.3 Correlation of Stress with Y-Q calculated from Rwd

The Multi-Body Simulation (MBS) for Railway Dynamics (RWD) calculation provides numeric models that can be used to evaluate Y and Q forces applied on each wheel of the bogie. The calculation considers the train characteristics (such as bogie position in train) and the track characteristics (such as curve radius and friction coefficient).

All the simulation parameters in the identified curves (3,4,5, respectively WB240, WB220 and WB110) are known except for friction coefficient. Y and Q forces values can be calculated and then provided to FE calculation for comparison of stresses between on track test and FE calculation.

*Note: Another Y & Q forces estimation by empirical method was carried out on a test bench. The test was abandoned due to aberrant results mainly related to the specific boundary condition of the test. See Appendix 1.*

The correlation with FEM calculation and stress measurements gives confidence on the relation between

- Y & Q input for Railway Dynamics (Rwd) quasi-static calculation in several curve
- R12:a, R10:c On-track measurement on same curves

We were then able to identify a quasi-static relation between "R12:a" and loads Y & Q:

$$R12 :a Mx-Mn = a_Y * Y + a_Q (Q0 + dQ)$$

and  $(R12:a Mx-Mn)_{mean} = a_Q * Q0$  due to zero of strain gauges in straight line

So finally, the  $Y = f^{-1}(\sigma_{R12})$  function was determined as:

$$Y = (R12:a Mx-Mn - (R12:a Mx-Mn)_{mean} - a_Q * dQ) / a_Y$$

*Note: "dQ" (dynamic variation of vertical loads) cannot be measured. We considered 10 kN as a conventional value on this type of curves with this material (according to Railway Dynamic Calculation). The "a\_Q \* dQ/a\_Y" is a corrective term in the equation with an impact of 1,66 kN on the Y value.*

The statistical analysis in wheel turn can give the "Exceptional" and "Fatigue" levels to be considered per load case. This led to an estimation of the maximum and average Y quasi-static load for the whole run based on "R12.a" measurement.

Weighting of AW0/AW3 occurrence should be taken into account for fatigue value, Figure 15.

Effort Y[kN] (a <sub>Y</sub> =8.4, a <sub>Q</sub> =1.4, dQ = 10)		
SUMMARY	AW0	AW3
max	46,5	51,4
q99.85	36	47,4

→ Exceptional  
 → Fatigue

**Figure 15 – Results extracted from the statistical analysis**

The Y quasi static load used during the design was based on the equations defined in the EN13979-1 (European standard for technical approval of monobloc wheels) [P2]. This standard defines the loading conditions to be considered for both Exceptional and Fatigue conditions.

For transversal Y quasi static loads, the comparison is shown below:

	Y [kN]	
	EN 13979-1	Measurement 2022
Exceptional	52.5	51.4
Fatigue	42.3	47.4

**Figure 16 – Fatigue cases: Comparison of the transversal loads**

For the test performed in 2022, this comparison clearly shows that, for the exceptional conditions, the design hypotheses seem to fully cover the loads coming from the track.

For fatigue conditions (in AW3 load state), the loads coming from the track can be up to 12% higher than the load values considered for the design of the solution. This AW3 load was used during the test to cover the full design envelope. In Ottawa, during operation, the maximum passenger load is closer to AW2 load state, leading to reduce the real wheel loads compared to AW3.

In any case, this means that the fatigue load supported by the assembly in service are close to the design limit if not above.

Such levels of transversal loads correspond to a high friction coefficient of 0,5. This theoretical value being hard to be measured and monitored directly, it is important to reduce it as much assuming the following conditions are met:

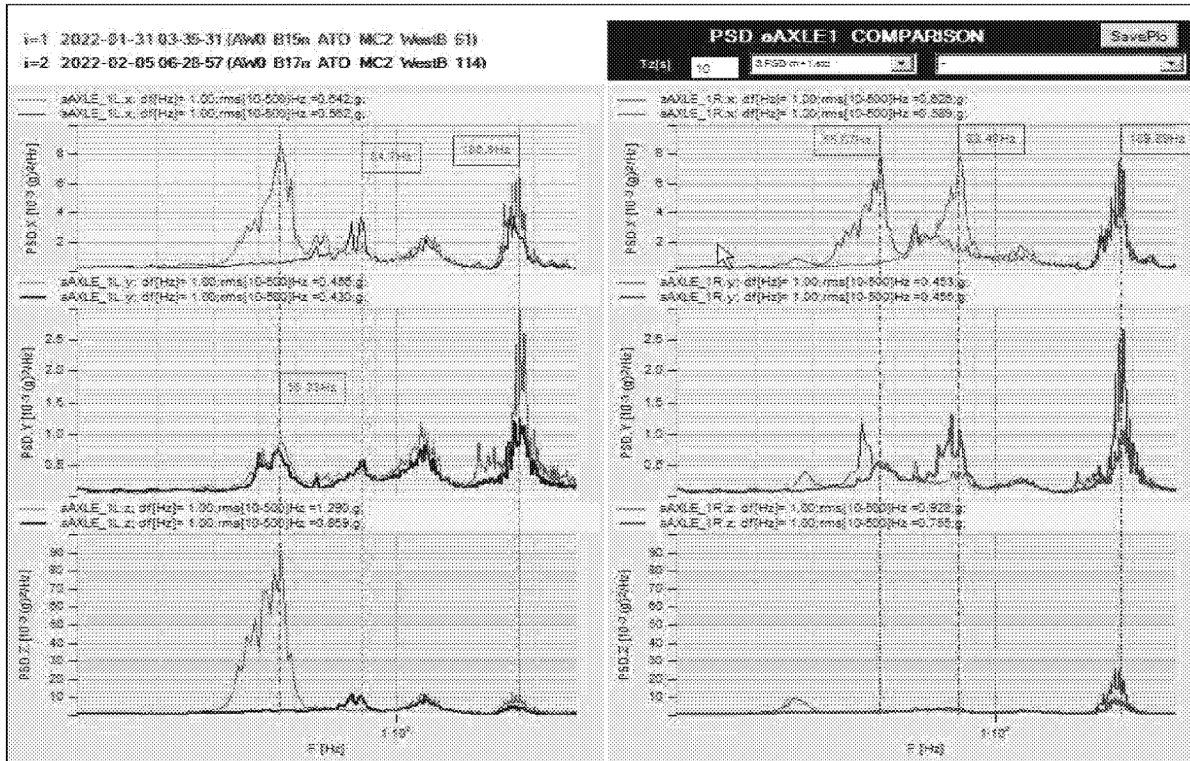
- a proper surface condition of the track (specifically rail profile, cant, corrugation, flatness...)
- a proper surface condition of the wheel (specifically sharp edge on the flange, hollowing...)
- a proper lubrication of the rail/wheel flange

### **3.1.4 Influence of wheel/rail contact (B15 / B17 profile)**

To quantify the impact of track geometry and wheel/rail contact, an alternative wheel profile (B17) was also tested

PSD comparison (Figure 17) of leading axle boxes acceleration showed that enlarged track clearance with B17 profile, compared to B15 profile, leads to less coupling in X-Z direction with Y solicitation in curve on disk brake side (55 Hz).





**Figure 17 - Comparison between B15 and B17 measurement**

The following table summarizes the on-track data (stress in R12 and small bearing section on hub) under different conditions:

Max Mn / wheel turn	AXLE2- Brake2R side - R12										Small Bearing - c (tangential)									
	SigmBrk2R_R12_0_a_MkMn[Mpa]					SigmBrk2R_R12_180_a_MkMn[Mpa]					SigmBrk2R_R120_c_MkMn[Mpa]				SigmBrk2R_R180_c_MkMn[Mpa]					
Config	mean	max	q99.85	q95	m-3std	mean	max	q99.85	q95	m-3std	mean	max	q99.85	q95	m-3std	mean	max	q99.85	q95	m-3std
AWO-B15w	72,7	499,8	396,6	210,2	255,8	85	506,1	430,9	241,7	293,7	26	161,2	130,4	71,3	83,8	23,1	135,9	117,9	66,6	77,6
AWO-B15n	74,4	509,1	421,6	229,7	272,7	81,6	505,1	448,6	242,9	296,9	25,5	158,9	132,9	73,2	86,2	22,9	141,6	123,3	66,9	77,8
AWO-B17	61,1	404,5	358,8	151,5	201,7	74	478,9	419,7	187,7	247,7	21,5	153,5	132,3	49,1	70,3	19,9	142,7	122,5	46,2	65,8
AWO-B17Flat	55,5	375,2	332,6	131,6	183,7	76,7	487,2	426,5	195,7	259,9	21,7	152,8	136	53,7	76,1	30,2	142,4	126	46,4	69,3
AW3-B15n	98,9	617,7	528,2	319,4	366,1	106,3	609,1	559,2	344	391,1	29,7	182,5	165,9	97,6	111,8	26,8	176,7	152,8	51,3	103,2

Max Mn / wheel turn	AXLE2- GearBOX 2L side - R12										Small Bearing - c (tangential)									
	SigmGear2L_R12_0_a_MkMn[Mpa]					SigmGear2L_R12_180_a_MkMn[Mpa]					SigmGear2L_R120_c_MkMn[Mpa]				SigmGear2L_R180_c_MkMn[Mpa]					
Config	mean	max	q99.85	q95	m-3std	mean	max	q99.85	q95	m-3std	mean	max	q99.85	q95	m-3std	mean	max	q99.85	q95	m-3std
AWO-B15w	88,6	417,9	378,9	194,2	247,4	86,3	422,8	386,3	193,5	247,7	24	150,3	125,1	58,9	77,5	27,9	143,9	118,7	57,4	74
AWO-B15n	87,8	471,1	408,3	283	298,6	87,5	506,1	418,3	262,6	299,9	24,8	167,9	139,3	80,7	94	28,6	155,6	127,1	76,4	88,2
AWO-B17	80,4	434,1	388,5	195,8	243,7	79,8	441,6	390,3	192,3	240,5	22,3	149,3	126,9	56,7	75,1	24	128,9	117,4	52,7	69,6
AWO-B17Flat	83,4	443,7	393,9	200,9	252	81,5	447,3	389,9	192,5	243,5	26,1	157,2	125,6	80,4	79,5	23,8	130,9	118,7	55,8	72,6
AW3-B15n	112,2	589,2	539,1	337,4	387,3	110,3	593,3	546,6	337,4	388,5	28,6	215,2	179,1	99,1	115,7	30,3	200,1	159	93,5	107,3

**Figure 18 On track measurement results in different runs**

Comparing same operating conditions in AWO load condition, we can see that an alternative B17 profile would lead to reduce the level of stresses in the assembly both in the R12 area and the bearing seat (up to 20%) in comparison to a B15 new profile (B15n)

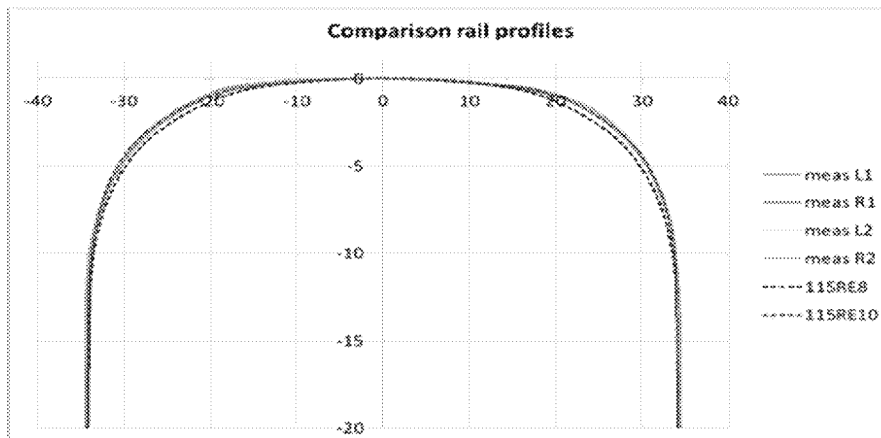
There are two aspects of the interface between wheel and rail profile that need to be highlighted, in terms of why an alternate profile is being considered,

UNCONTROLLED WHEN PRINTED – Not to be used before verification of applicable version number

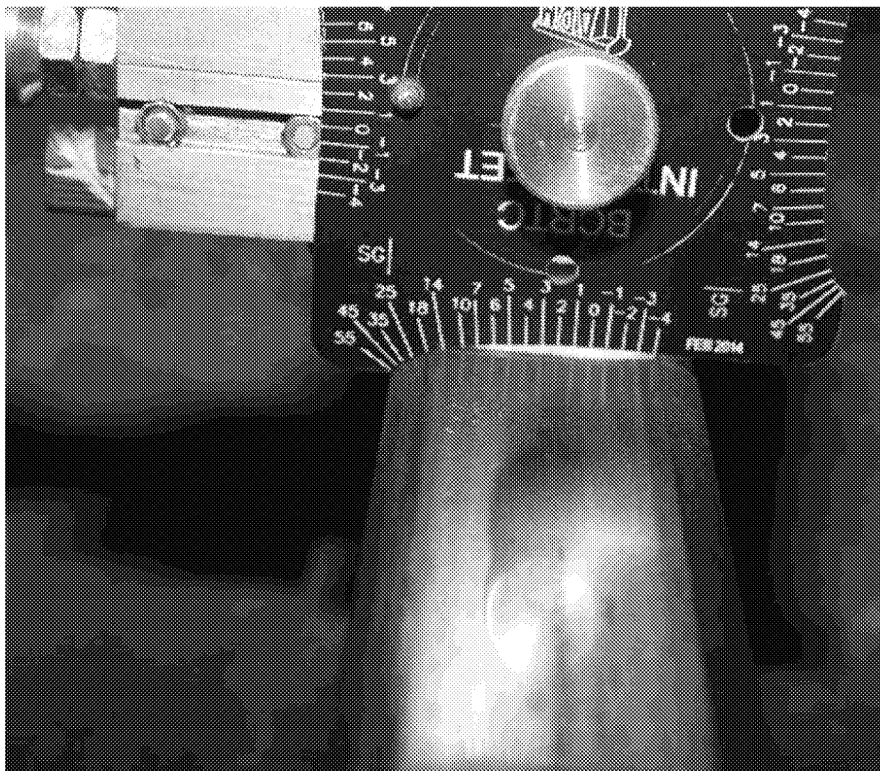
**“CONFIDENTIAL -TRADE SECRET” - © ALSTOM SA 2020. All rights reserved. Reproduction, use or disclosure to third parties, without express written authorisation, is strictly prohibited.**



- As part of the investigation into the yard derailment of TS16, the question of the rail profile being a contributor to the derailment was raised. At that time, using the Calipri™ tool to measure a new section of rail, it was found that the rail cross section did not match the specified 115RE 8 inch crown rail. The profile comparison is shown below



- In addition, as part of the re-machining process for the rails, an initial survey was conducted by the subcontractor, The profile is shown below



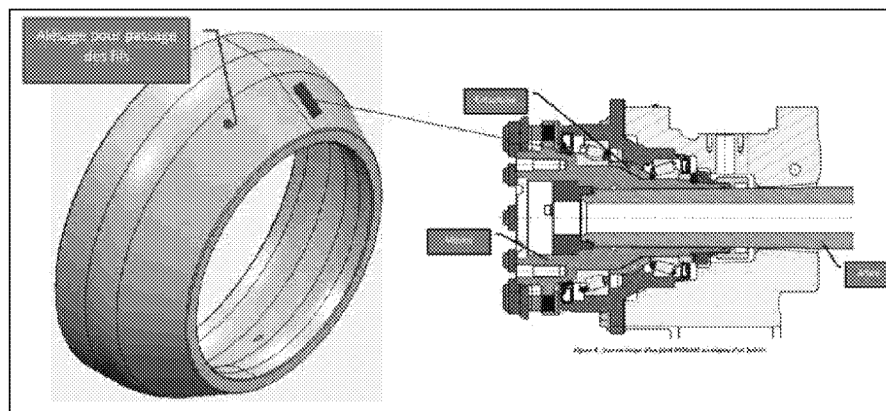
The reported conclusion was that this profile could not have occurred naturally, but the subcontractor did not have sufficient history of the track to explain the condition. It is known that prior to the start of service there was a surface grinding operation to remove surface corrugation, prior to the start of revenue service.

*UNCONTROLLED WHEN PRINTED – Not to be used before verification of applicable version number*

**“CONFIDENTIAL -TRADE SECRET” - © ALSTOM SA 2020. All rights reserved. Reproduction, use or disclosure to third parties, without express written authorisation, is strictly prohibited.**

### 3.1.5 Bearing Spacer Rotation

The bearing spacer was instrumented with strain gauges, Figure 19. On track data, the log did not show sensibility to forces in curve but showed brutal loss of signal from spacer after 70km test run. This would suggest part movement in the assembly. The phenomenon needs to be confirmed by the teardown on the test parts.



**Figure 19 - Instrumented bearing spacer**



### 3.1.6 Comparison track quality with 01/2021 test

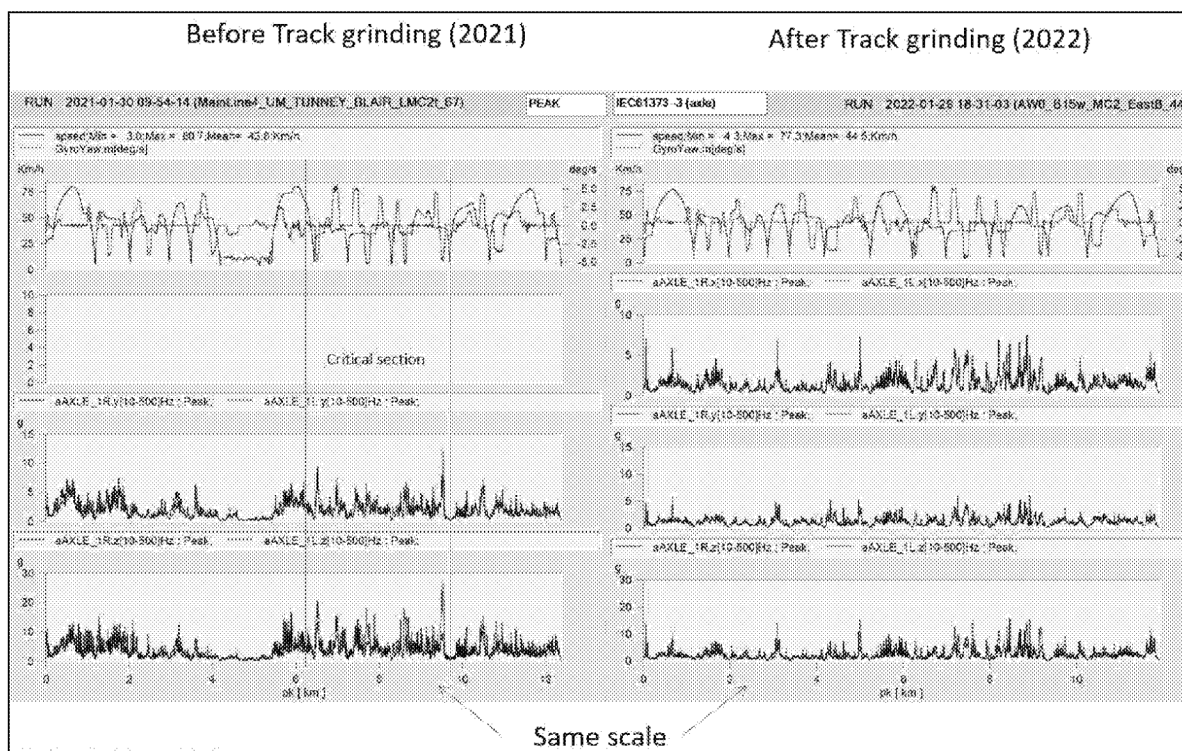
Track excitation of vehicle was evaluated through axlebox acceleration measurement, performed at different periods of time on the track:

- January 2021 on LRV26 (Starting date, 30/01/2001)
- January 2022 on LRV15 (Starting date, 29/01/2022)

In both cases :

- vehicle was in tare (AW0)
- running on East Bound (Tunney → Blair)
- with LMC2 leading (axle1 of BM3 is the leading axle of bogie), which is the most sensitive case in term of lateral track forces.

Measurements taken after track grinding show peak axle box accelerations (calculated on 10m window, within [10-500] Hz) were reduced by a factor 2 in curves: in vertical **and also in lateral direction** compared to the same measurements before grinding.



**Figure 20 - Comparison of 2021 VS 2022 Peak acceleration level on axle box**

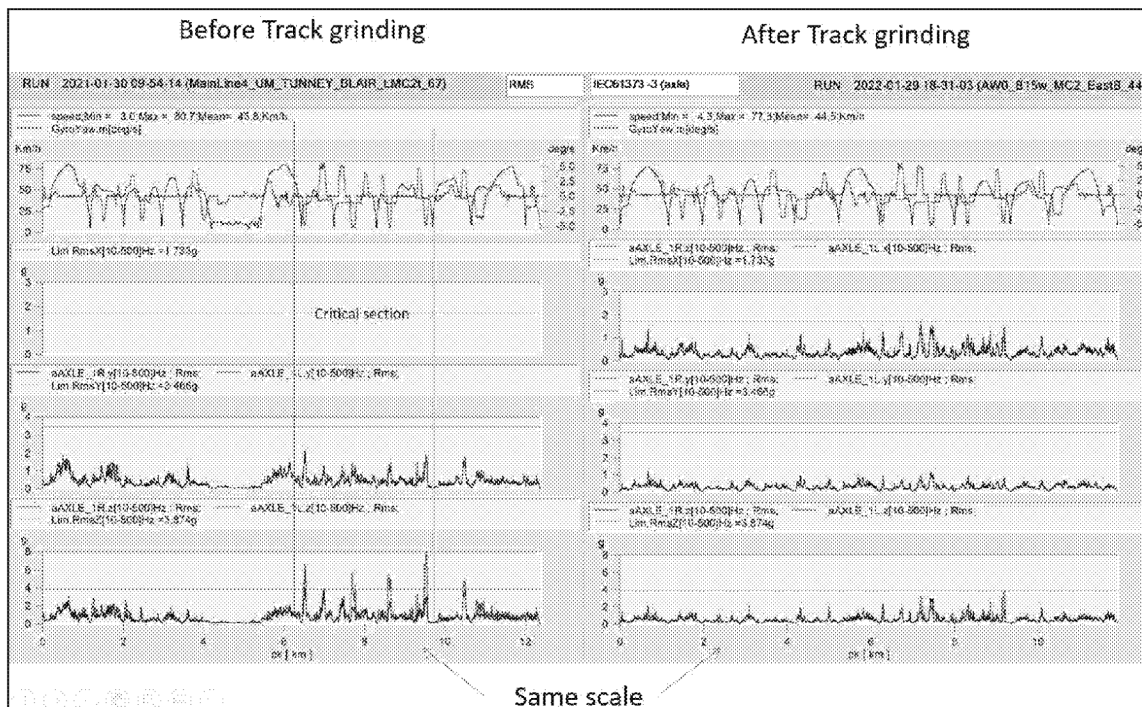
The RMS axle box accelerations (calculated on 10m window, [10-500] Hz), clearly demonstrated an excessive level in curve section, and coupling with lateral excitation in 2021, Figure 21.

Note that, RMS value in the worst areas exceed IEC61373-3 [P3] guideline.

UNCONTROLLED WHEN PRINTED – Not to be used before verification of applicable version number

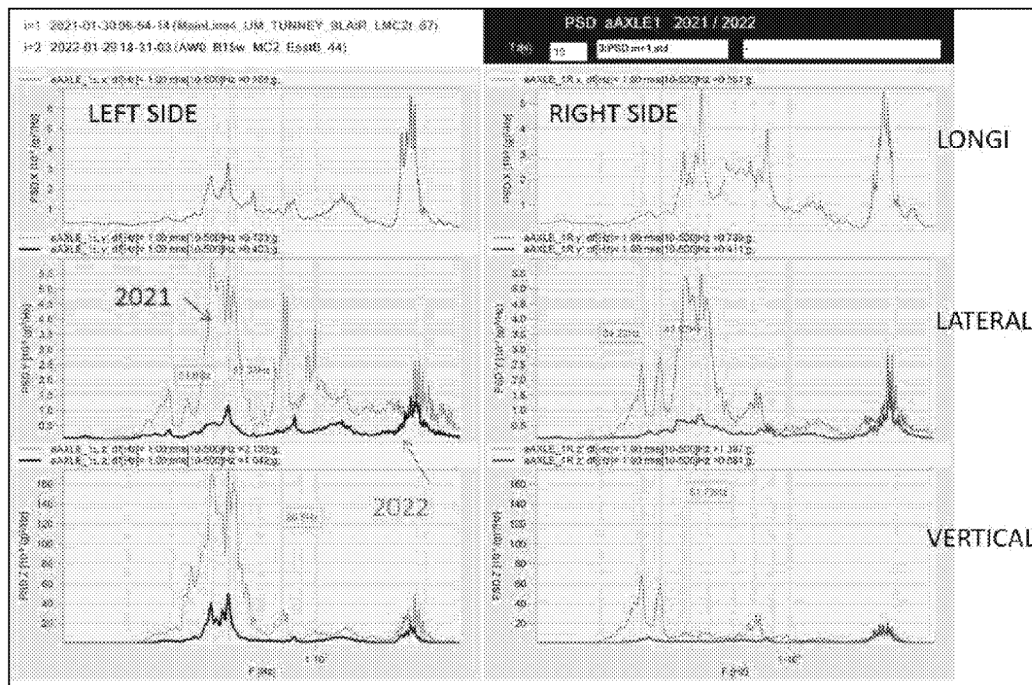
**“CONFIDENTIAL - TRADE SECRET” - © ALSTOM SA 2020. All rights reserved. Reproduction, use or disclosure to third parties, without express written authorisation, is strictly prohibited.**





**Figure 21 - Comparison 2021 VS 2022 RMS acceleration level on axle box**

The PSD (Power Spectral Density) axle box accelerations analysis, cumulating a “10 seconds” window along the track and retaining spectrum envelop as a “Mean+1 standard deviation”, points out vertical excitation on 2021 related to top of rail corrugation **but also increased lateral excitation which is sensitive for the bearing of the CBA as demonstrated previously, Figure 22.**



**Figure 22 - Comparison 2021 VS 2022 PSD analysis**

UNCONTROLLED WHEN PRINTED – Not to be used before verification of applicable version number

**“CONFIDENTIAL - TRADE SECRET” - © ALSTOM SA 2020. All rights reserved. Reproduction, use or disclosure to third parties, without express written authorisation, is strictly prohibited.**



Calculation of RMS Value in [10 – 500] Hz confirms a **significant amplification of vertical but also lateral axle box acceleration** due to track quality.

RMS level [10-500] Hz, PSD m+1std, values are expressed in g				
BM5 – LMC2, axle 1 <i>leading axle to East Bound</i>	LEFT SIDE		RIGHT SIDE	
	2021	2022	2021	2022
LATERAL (Y) (g)	0,733 <b>(+81%)</b>	0,403	0,739 <b>(+79%)</b>	0,411
VERTICAL (Z) (g)	2,136 <b>(+104%)</b>	1,402	1,397 <b>(+62%)</b>	0,861

**Figure 23 - East Bound Track RMS comparison 2021 VS 2022 (results expressed in g)**

The measurement showed much higher acceleration level on axle box in 2021 in both lateral and vertical directions. It also gave abnormal noisy feeling in vehicle in 2021. Reduction of vibrations and excitations from track will be of course favorable for the mechanical system and could avoid damaging the system.

This can be once again monitored by:

- Wheel/rail profile maintenance strategy
- Lubrification focus to reduce friction in curve

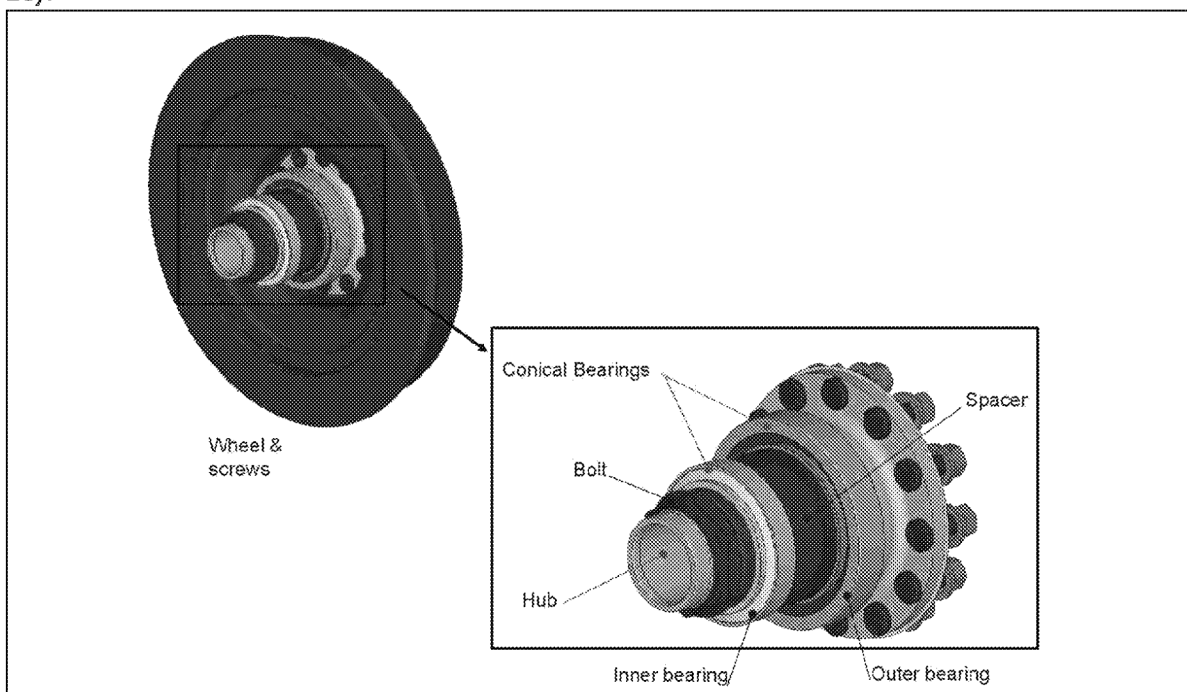
## 3.2 Finite Element Analysis

### 3.2.1 Calculation model

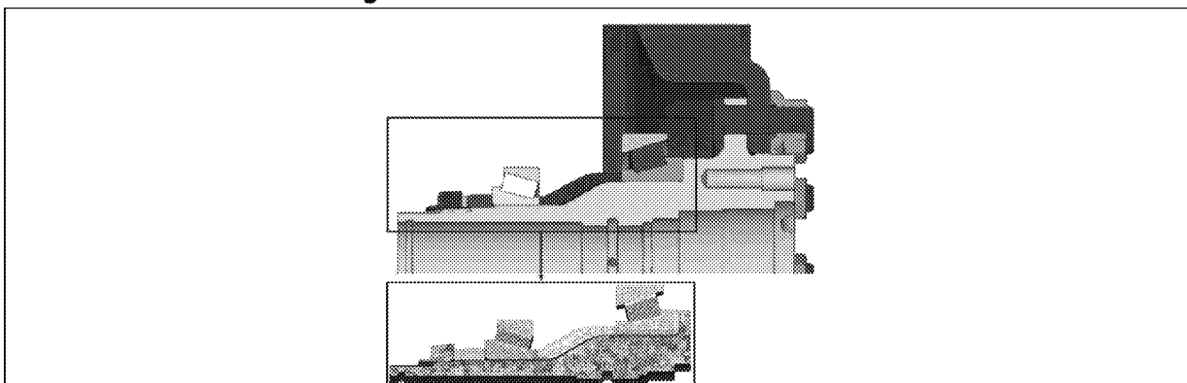
A Finite Element Model (FEM) of the assembly of the axle hub was built. This model takes into account all the components of the direct environment of the hub, i.e.:

- the wheel, that allows the track loads application,
- the screws,
- the conical bearings,
- the spacers,
- the bolt.

The following picture (Figure 24) presents two visualizations of the complete model, in the isometric point of view and along a cut section. A detailed view of the mesh is also presented in the cut section (Figure 25).



**Figure 24 - Global overview of the FE model**



**Figure 25 - Cut section of the numerical model**

*UNCONTROLLED WHEN PRINTED – Not to be used before verification of applicable version number*

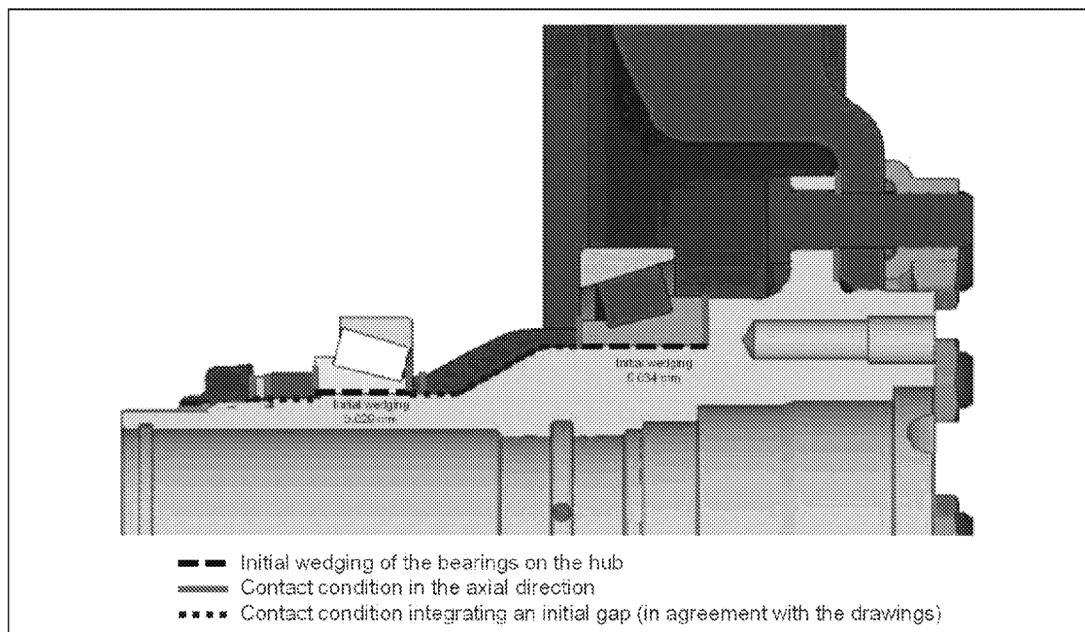
**“CONFIDENTIAL - TRADE SECRET” - © ALSTOM SA 2020. All rights reserved. Reproduction, use or disclosure to third parties, without express written authorisation, is strictly prohibited.**



The complete model is composed of 3.3 million nodes and 2.2 million elements.

All the components of this assembly are made of various steel alloy grades. The behavior of these components is assumed to be linear elastic. Usual mechanical properties are therefore considered in all the numerical simulations that were run: Young's Modulus  $E = 210\,000\text{ MPa}$ , and Poisson's ratio  $\nu = 0.3$ .

In order to be as representative as possible, all the interfaces between the different components are modelled though contact conditions with friction coefficient, including the initial gaps or wedgings (according to the drawings). The Figure 26 below details the contact conditions.



**Figure 26 - Contact conditions applied to the interfaces**

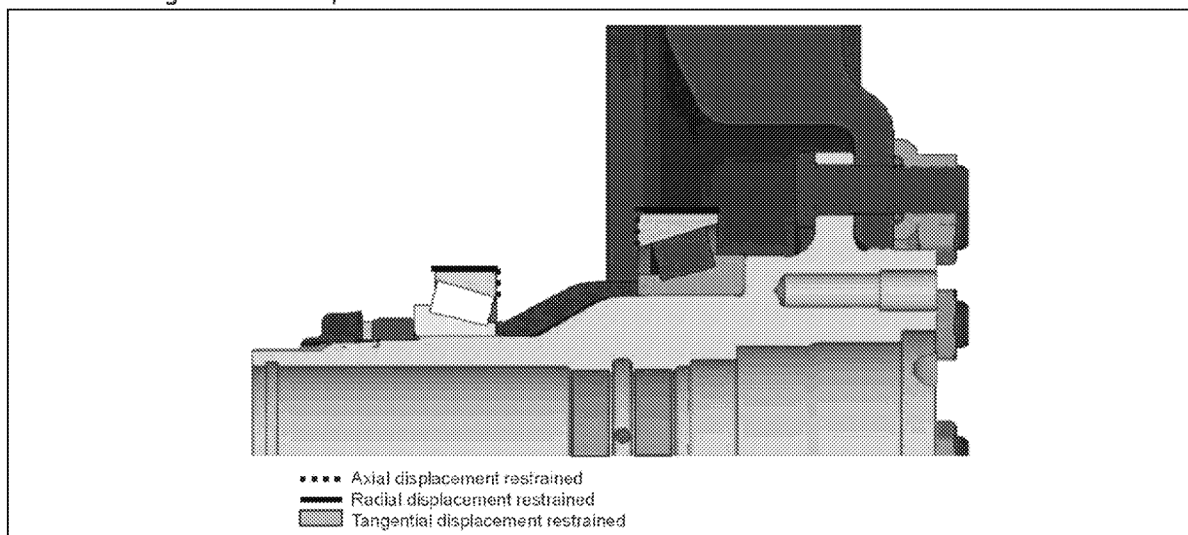
The model is restrained on the following areas:

- The outer rings of both bearings: axial and radial displacements are restrained on the surfaces that are lying along the axle beam,
- The tangential displacement of the hub is restrained at the splines to avoid free rotation around its own axis.

*UNCONTROLLED WHEN PRINTED – Not to be used before verification of applicable version number*

**“CONFIDENTIAL -TRADE SECRET” - © ALSTOM SA 2020. All rights reserved. Reproduction, use or disclosure to third parties, without express written authorisation, is strictly prohibited.**

The restraining surfaces are presented below:

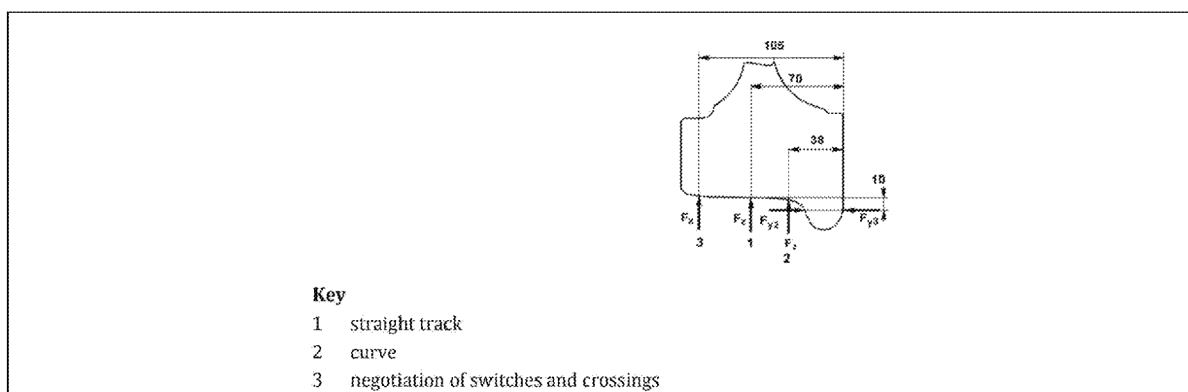


**Figure 27 – Overview of the boundary conditions**

One of the main points of attention is the bearings modelling. The conical rolling elements are simplified through a torus, with specific material properties. More details about this modelling are given in the next section.

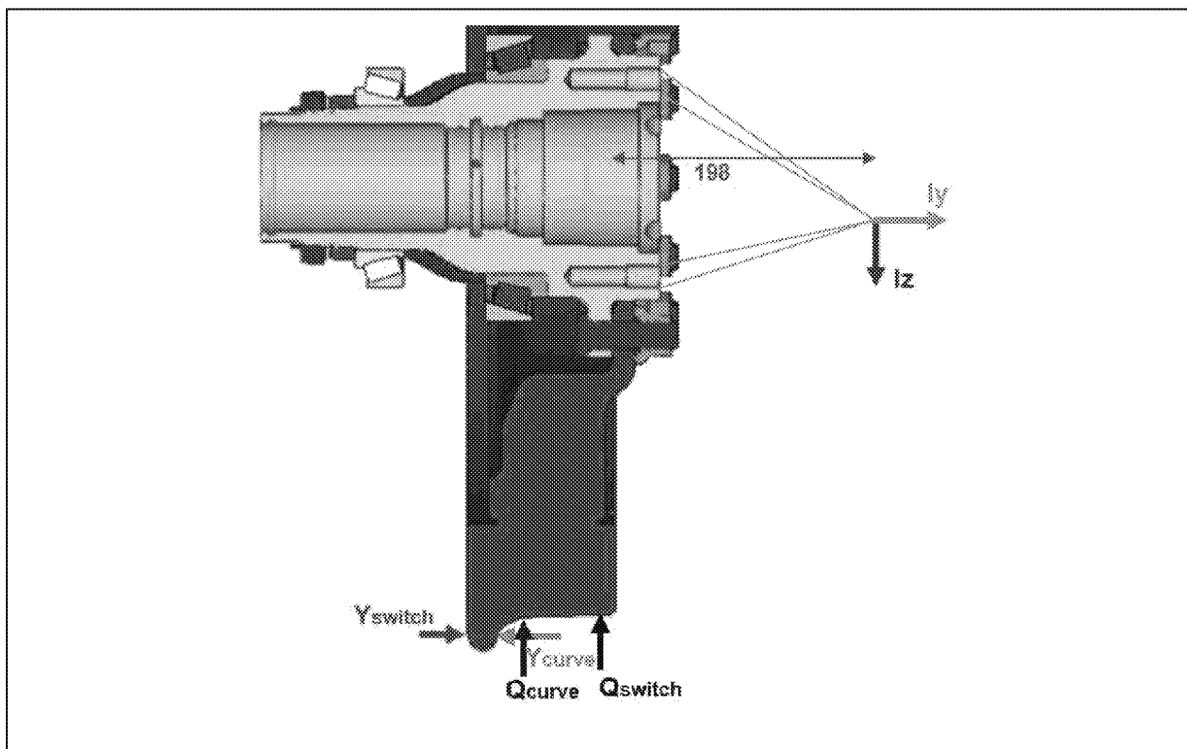
The next figure details all the points where the loads are introduced in the model:

- Transversal and vertical loads (respectively Y and Q) are applied at the wheel/rail contact point, as presented in the below figure. The combination of Y and Q loads are representative of the circulation of a vehicle on the track, either in a curve ( $Q_{curve}$  &  $Y_{curve}$ ), or in a switch ( $Q_{switch}$  &  $Y_{switch}$ ). The position of the points where the curve and switch loadings are applied is defined according to the recommendations of the EN13979-1[P2] (see Figure 28).
- The influence of the inertia of the gearbox is also investigated (loads  $I_y$  and  $I_z$  are applied at the center of gravity of the gearbox) (see Figure 29)



**Figure 28 – Wheel/track load introduction points – Extract from EN 13979-1**





**Figure 29 – Applied loads description on the FEM**

UNCONTROLLED WHEN PRINTED – Not to be used before verification of applicable version number

**“CONFIDENTIAL - TRADE SECRET” - © ALSTOM SA 2020. All rights reserved. Reproduction, use or disclosure to third parties, without express written authorisation, is strictly prohibited.**

### 3.2.2 Key parameters & hypotheses

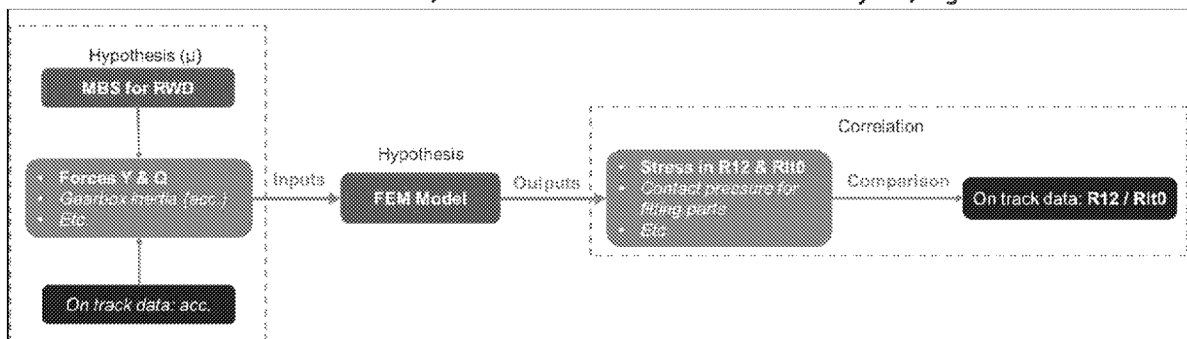
As described in the above section, the numerical model presents many non-linearities, mainly due to the numerous contact conditions that need to be solved. Such kind of model requires important computing resources (CPU, memory...) and is time consuming. In order to avoid useless complexity (without degrading the quality of the results in the area of interest), certain assumptions have been made for purposes of the model.

The first assumption is relative to the wheel. The model has been built by considering a rigid wheel, i.e. without any rubber element. Nevertheless, the impact of this assumption on the results should be limited since:

- The diameter of the wheel corresponds to the diameter of a new wheel operated on Ottawa network.
- The locations of the points where the vertical and transversal loads are in line with the standards for wheel design and validation. Therefore, the generated moments in the hub are valid.
- The interface between the wheel and the axle hub is respected (in terms of stiffnesses, contact conditions and pretension of the screws), therefore loads are correctly transferred to the hub.

The second assumption that was made was with respect to the modeling approach used to develop an accurate estimation of the stiffness of both conical bearings, specifically, the contact conditions to be defined between inner and outer rings of each bearing in order to reduce the complexity of the numerical model. The rolling elements are simplified by a torus where orthotropic properties are applied. Mechanical characteristics of both tori are determined in order to correlate the radial and axial stiffnesses.

The main input of the FE model is the vertical and transversal loads applied at the contact between the wheel and the rail. Since the measurement of these loads at the wheel is not possible on track, Multi Bodies Simulations (MBS) have been used to assess, under the right load state, the loads coming from the track in alignment and in curves. These loads are introduced in the numerical model. As a result, to correlate the on-track measurements, the stresses in R12 location are analyzed, Figure 30.



**Figure 30 – Workflow for comparing stresses from measurements and calculations**



### 3.2.3 Calculation results

All the load cases (curve, switch and gearbox inertia) were run in order to analyse the behavior of the assembly when subject to external loads. Key findings were extracted from the numerical simulations. All these numerical analyses were run prior to the test campaign especially in order to drive the hub instrumentation (location and orientation of the gauges).

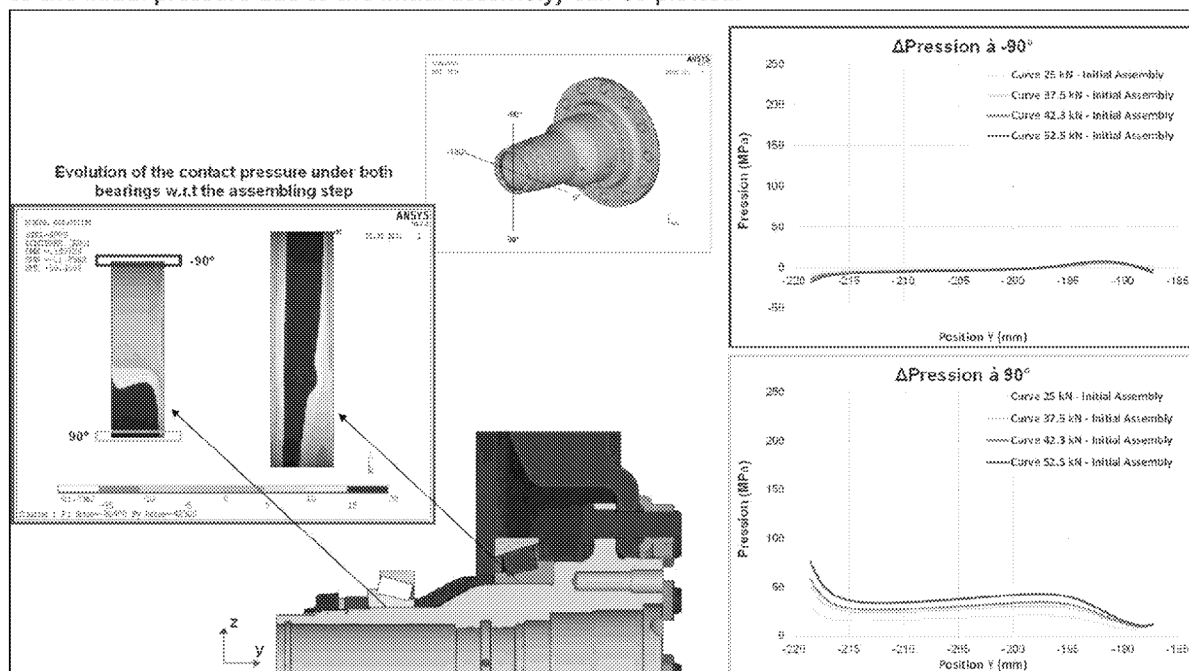
A specific attention has been paid to compare the differences between the contact areas between both bearings and the axle hub. This aimed to evaluate the following points:

- Contact pressure evolution versus wheel load conditions
- Potential loss of contact between the bearing ring and the hub
- Hub deformation under load
- Potential micromovement at the bearing fit interface

The analysis of the contact status (pressure, gap) was performed for both bearings. However, since the inner one is the most critical one, this section deals only with results related to the small bearing.

#### *Impact of the transversal load (Y Effort)*

The next figure (Figure 31) presents an interesting comparison on several results obtained with all the numerical simulations. The impact of four various configurations of transversal loads (from 25 kN to 52 kN) is analysed in terms of contact pressure. The numerical results allow to easily identify the areas where the contact pressure is increased or reduced. In addition, the variation of the contact pressure (with respect to the initial pressure due to the initial assembly) can be plotted.



**Figure 31 – Curve load case – Evolution of the contact pressure depending on curve loads**

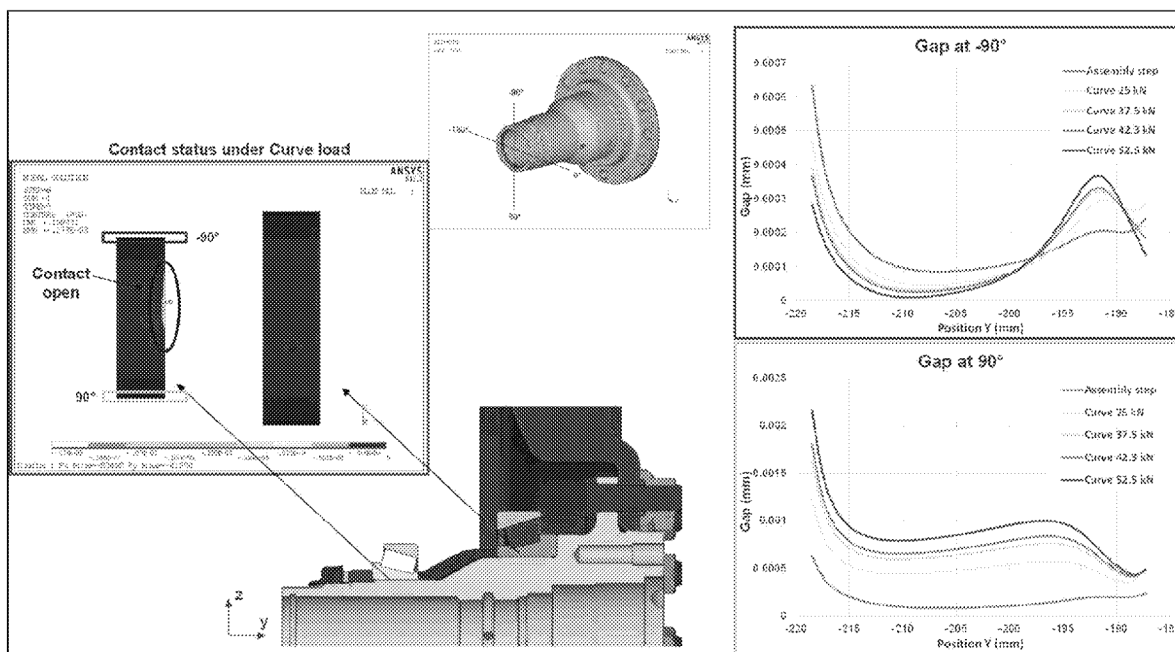
For the small bearing, the results clearly highlight that the contact pressure increases in the area close to the position +90° and reduces at the opposite side. The variation of contact pressure is also directly linked

UNCONTROLLED WHEN PRINTED – Not to be used before verification of applicable version number

**“CONFIDENTIAL - TRADE SECRET” - © ALSTOM SA 2020. All rights reserved. Reproduction, use or disclosure to third parties, without express written authorisation, is strictly prohibited.**

to the transversal load applied at the wheel: the higher the transversal load, the higher the variation of contact pressure (increase or reduction).

The next figure (Figure 32) illustrates the evolution of the gap between the hub and the small bearing for all load cases (after assembly, and after application of the curve loads). A positive gap value means that there is some interference, while a negative value means that there is some free gap (and therefore an open contact). On the image on the left-hand side of Figure 32 one can note a small area where the contact opens. Also, when the evolution of the gap is plotted for different angular positions ( $-90^\circ$  and  $+90^\circ$ ), one can see that, at the location  $-90^\circ$ , the gap decreases to almost 0 (meaning that all the interference due to the assembly is fully consumed) when the maximal Y load of 52 kN is applied.



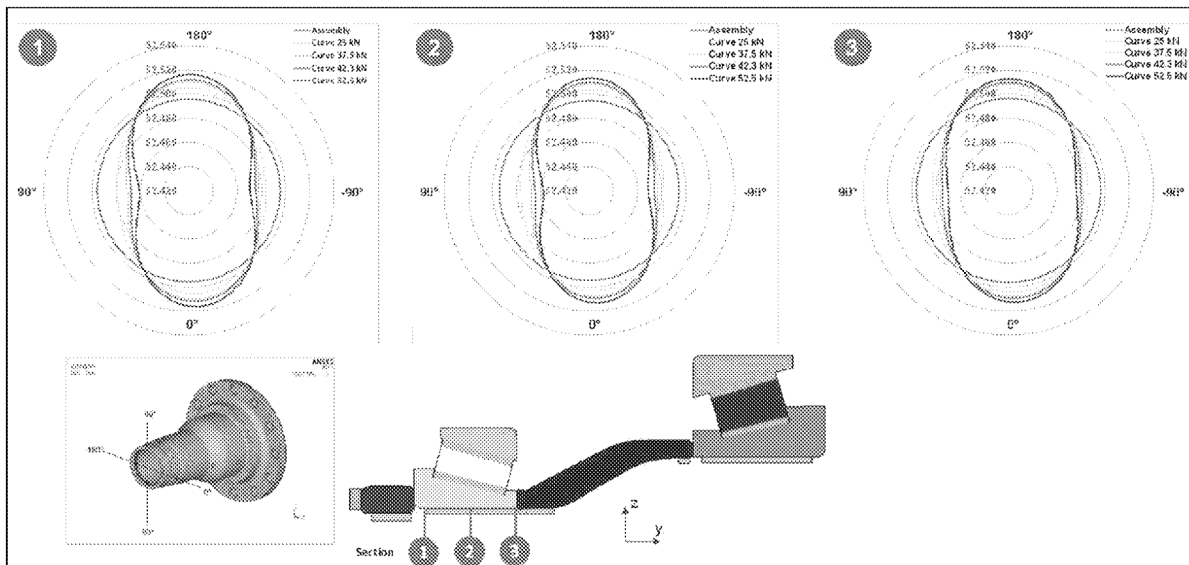
These two figures clearly show that, at the interface between the hub and the inner ring of the small bearing, the contact can evolve depending on the level of transversal load coming from the track.

In addition to the analysis of the contact details (status, pressure), it is also interesting to get an overview of the deformed shape of different sections of the hub (under the inner ring of the small bearing). In order to facilitate the comparisons and the analysis of the deformed sections, the center of the deformed shape is shifted back to zero. The figure below (Figure 33) shows that the hub becomes oval when the curve load (mainly Y effort) is applied.

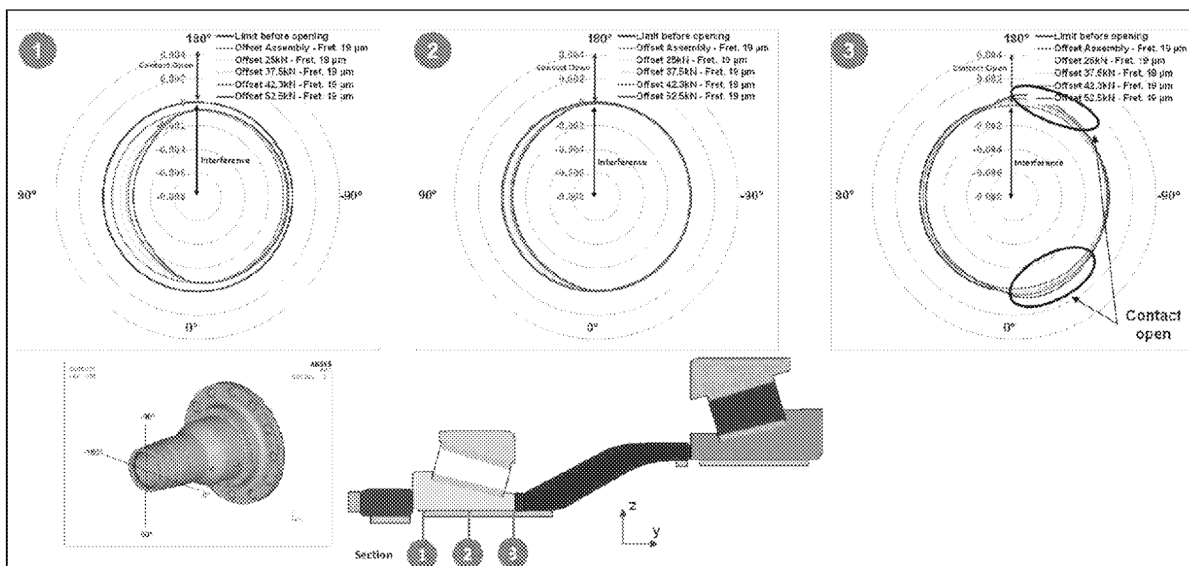
UNCONTROLLED WHEN PRINTED – Not to be used before verification of applicable version number

**"CONFIDENTIAL - TRADE SECRET"** - © ALSTOM SA 2020. All rights reserved. Reproduction, use or disclosure to third parties, without express written authorisation, is strictly prohibited.





**Figure 33 – Curve load case – Visualisation of the deformed shape under the small bearing**



**Figure 34 – Curve load case – Analysis of the areas of contact loss**

The above Figure 34 presents, for three sections, the angular evolution of the interference/gap between the hub and the inner ring. The red curve corresponds to a “no contact/no clearance” point, meaning that the contact is open for angular sectors where values are positive. This figure shows that the section 3 is the first one where the contact opens (this is another illustration of what has been presented in Figure 32). For this section, the contact opens on two areas (blue circles) as soon as the transversal load  $Y$  exceeds 37 kN. Because of the deformation of the hub, of the inner ring and the contact opening, there is some micro-displacement that could be generated between the bearing and the hub.

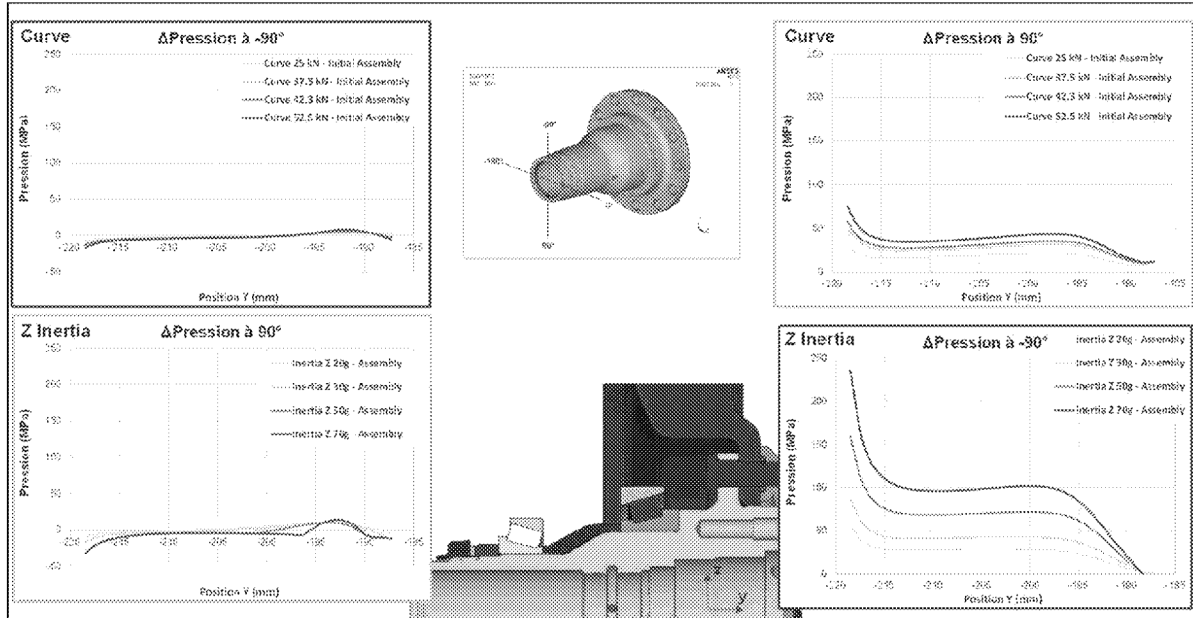
UNCONTROLLED WHEN PRINTED – Not to be used before verification of applicable version number

“CONFIDENTIAL - TRADE SECRET” - © ALSTOM SA 2020. All rights reserved. Reproduction, use or disclosure to third parties, without express written authorisation, is strictly prohibited.

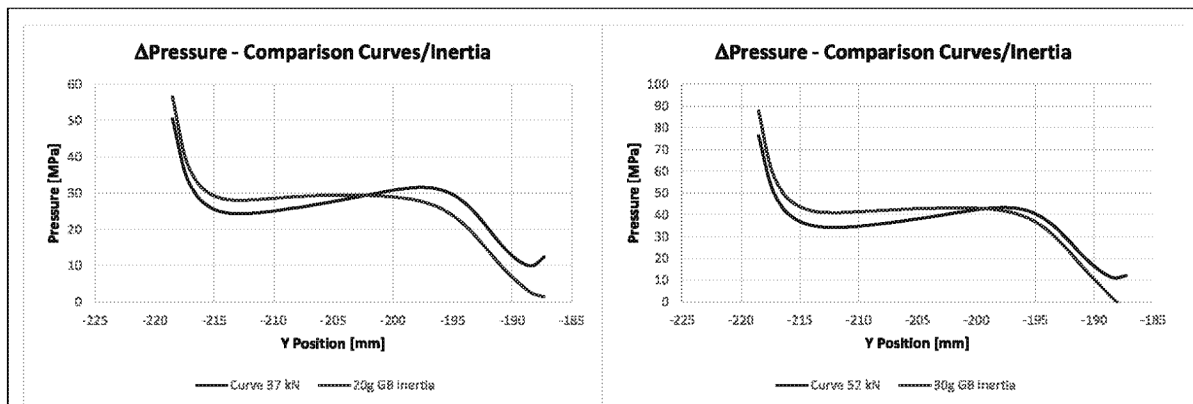
**Impact of the gearbox inertia**

A similar analysis was run for the gearbox inertia load cases, as set out in Figure 35. Four levels of vertical acceleration, from 20g to 70g (applied to the gearbox mass of 270 kg), were investigated in order to analyse the impact on the contact conditions and on the hub deformation. In both of the following figures, the comparisons of the variation of contact pressures and of the gap are presented.

The increase of contact pressure is consistent across both load cases (see Figure 36).



**Figure 35 – Gearbox Inertia – Variation of the contact pressure – Comparison with Curves cases**

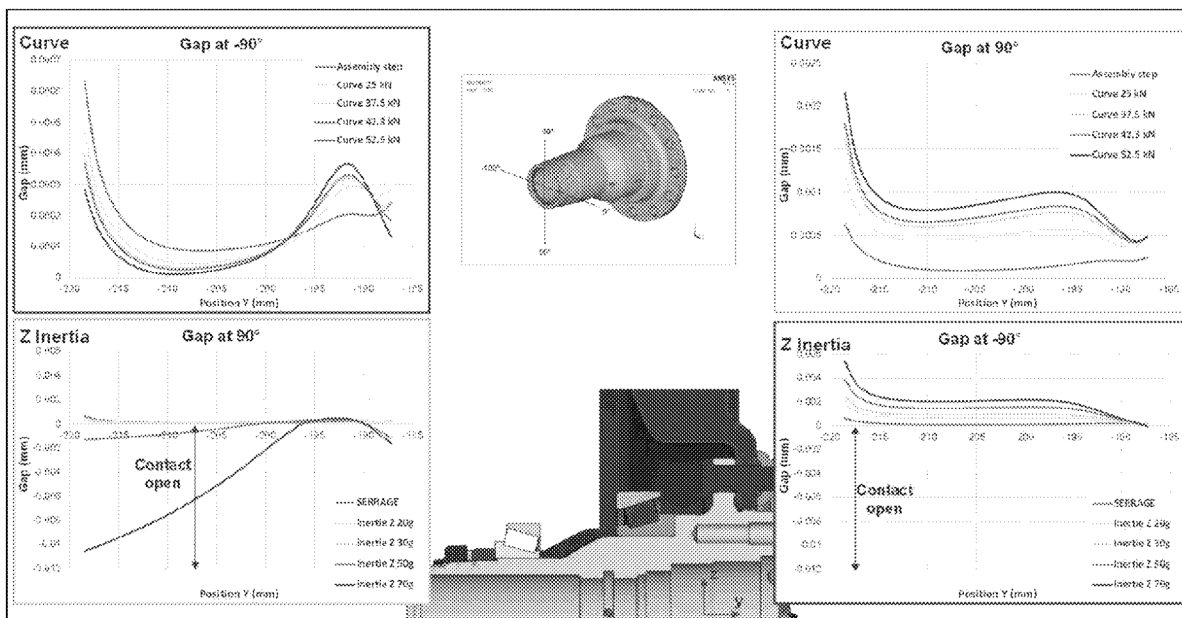


**Figure 36 – Comparison of the variation of contact pressure for Curves and Gearbox Inertia**

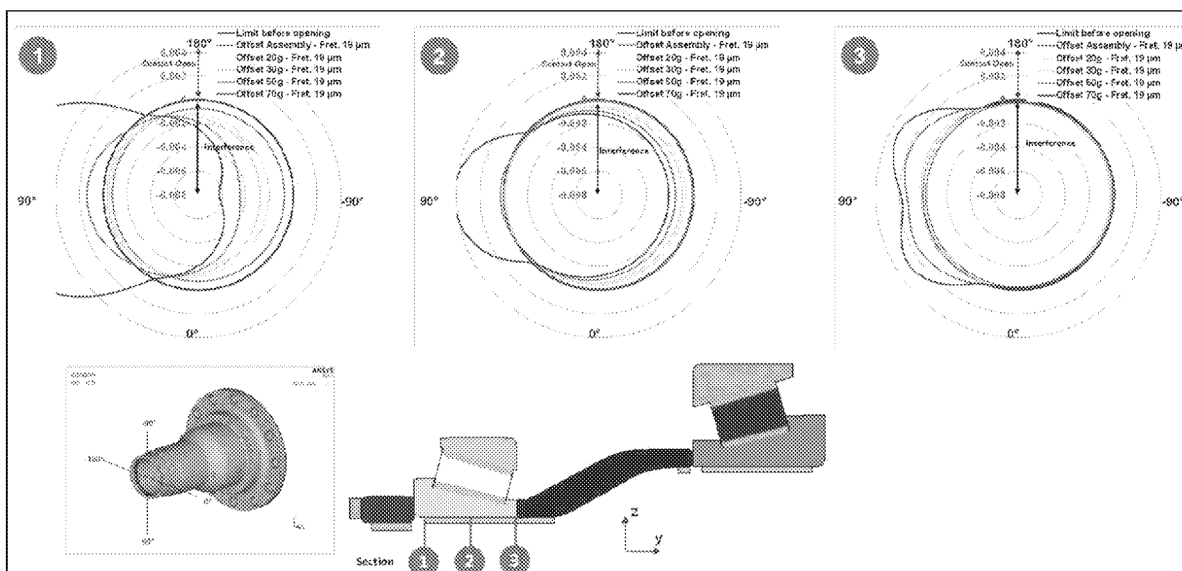
UNCONTROLLED WHEN PRINTED – Not to be used before verification of applicable version number

**“CONFIDENTIAL -TRADE SECRET” - © ALSTOM SA 2020. All rights reserved. Reproduction, use or disclosure to third parties, without express written authorisation, is strictly prohibited.**





**Figure 37 – Gearbox Inertia – Evolution of the contact gap – Comparison with Curves cases**



**Figure 38 – Gearbox Inertia – Analysis of the areas of contact loss**

We can see that the variation (especially the increase) of contact pressure due to the gearbox vertical inertia can be larger than the one generated by the transversal loads due to a curve, the origin being held in the moment that is generated in the hub:

- Moment generated by an acceleration of 20g is slightly lower than the moment generated by a transversal load of 37 kN.
- Moment generated by an acceleration of 30g is close to the moment induced by a transversal load of 52 kN.

UNCONTROLLED WHEN PRINTED – Not to be used before verification of applicable version number

**“CONFIDENTIAL - TRADE SECRET” - © ALSTOM SA 2020. All rights reserved. Reproduction, use or disclosure to third parties, without express written authorisation, is strictly prohibited.**

These theoretical results must be taken with caution. Indeed, the calculation performed is “static” whereas most of the vertical acceleration seen by the gearbox are transitory. It is then difficult to make a direct link on the real impact during service. It is also important to note that during the test, the “flat” configuration did not lead to significantly affect the stress level within the hub (maybe due to the position of the flat onto the wheel profile). However, as described in section 3.1.6, the actual level of the acceleration is reduced in comparison to the very high levels recorded in 2021.

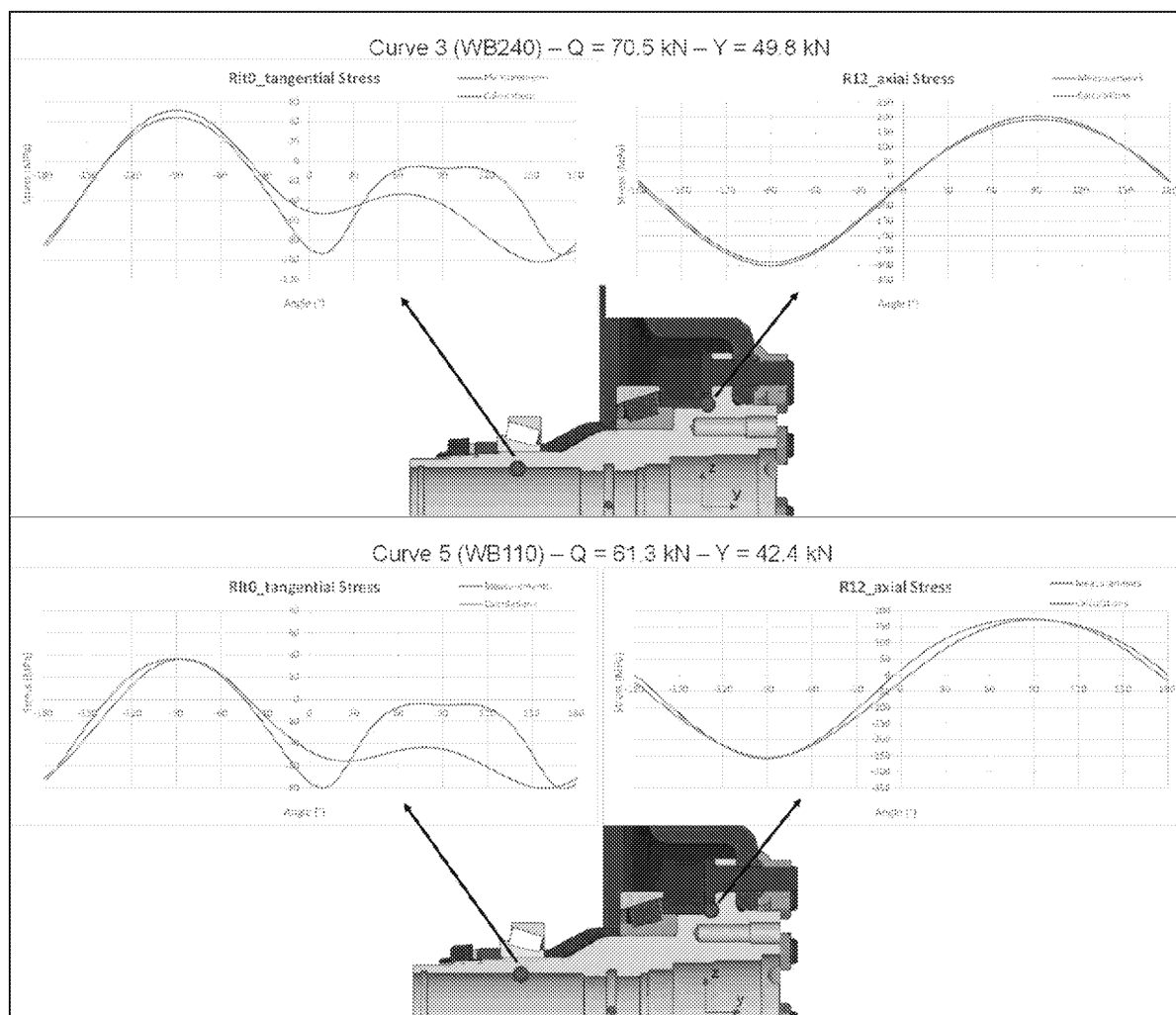
Therefore, it is still important to consider that the higher the vertical acceleration is (mainly due to track condition such as corrugation), the worse it could be for the axle integrity. A specific care needs to be given to the track quality.

**During the 2022 test campaign, the identified key factor was the transversal loads generated in curves.** In the following section, the comparison and correlation between the measurements and the calculation results will be discussed.



### 3.2.4 Correlation with test results

As explained in paragraph 3.1.3, vertical and transversal loads computed by Multi-Bodies Simulations are applied in the FE model for computing the stresses in both "R12" and "Rit0" locations. The graphs that are presented below (Figure 39) depict the evolution of the stresses for these two locations over one single wheel turn.



**Figure 39 – Measurements / Calculations – Stresses for R12 & Rit0 locations for Curves 3 & 5**

The analysis of the stress range (variation from minimal to maximal stress) at both locations was performed for numerical results and measurements, as set out in Figure 40.

		Stress Range [MPa]	
		R12	Rit0
Q = 61.3 kN Y = 42.4 kN	Calculation	428.9	117
	Measurement	433	116.7
Gap Measure/ Calculation [%]		1%	0%

UNCONTROLLED WHEN PRINTED – Not to be used before verification of applicable version number

**"CONFIDENTIAL - TRADE SECRET"** - © ALSTOM SA 2020. All rights reserved. Reproduction, use or disclosure to third parties, without express written authorisation, is strictly prohibited.

		Stress Range [MPa]		Ratio R12/Rt0
		R12	Rt0	
Q = 61.3 kN	Calculation	428.9	117	3.7
Y = 42.4 kN	Measurement	433	116.7	3.7
Q = 61.3 kN	Calculation	356.6	94.1	3.8
Y = 33.7 kN	Measurement	-	-	-
Q = 70.5 kN	Calculation	505	153	3.3
Y = 49.8 kN	Measurement	481	138	3.5

**Figure 40 – Measurements / Calculations – Link between the stresses in R12 and Rt0**

The above table reveals a high correlation between the FEM results and the measurements for the first couple of loads (Q=61.3 kN – Y=42.4 kN). The gap in terms of stress range is lower than 1% for both locations.

This table also shows that the numerical model is accurate to capture the level of stress computed at "Rt0" location with respect to the "R12" location. A factor close to 3.5 between the stresses at these two locations is computed and this factor is fully in-line with the observations made during the on-track tests. This factor is also confirmed for another set of loads. Further calculations are being performed on other data sets to confirm its global accuracy.

Given these first results, the FEM model is judged representative of what is measured on real hubs for quasi-static conditions.



### 3.3 Analytical approach

The aim of the analytical approach is to define key parameters associated to one or some criteria in order to identify a validity domain of the design under a certain level of loads.

From the parameters described in section 2.2.3, we will now be able to compare several criteria:

- A bearing supplier criterion. Very conservative and which doesn't take into account the material characteristics. The principle of this criterion is to define the minimum bearing interference fit, function of the bearing and shaft geometry and the external load. *Note: the bearing fitting cannot be too important to avoid damaging the bearing itself.*
- An analytical criterion based on a classical "Archard wear law" which could simply integrate the geometry, the micro-displacements (load related), material characteristics and wear typology we are facing (fretting in our case).
- A mechanical criterion based on the comparison between fatigue limit of material and surface stress induced by contact pressure, micro-displacement, and friction factor.  
It needs a complex and correlated FEM calculation (see 3.2.3). The advantage of such criterion is that it considers all the geometrical even if it still needs hypothesis on friction (value, stability, homogeneity).

Further analysis still needs to be carried out by comparing the design and application throughout different projects / product ranges without fretting concern, to refine the acceptance criterion to be considered.

These approaches combined with the correlated FEM model will enable us, if needed, to propose several design improvements to sustain the running conditions met in Ottawa network since the commissioning of the fleet.

## **SECTION 4 PRELIMINARY CONCLUSIONS & RECOMMENDATIONS**

### **4.1 Preliminary Conclusions & Further Investigations**

Based on the above analysis, the test and simulations showed that one of the key factors related to the fretting issue is the Y quasi-static loads mainly generated during curving. These loads are higher on the 2 bogies at the extremities of the trainset in the Ottawa trainset. This is mainly due to the more severe lateral forces on the extreme axes during operation, and also due to the higher nominal axle load. This is in line with the fleet control status showing a higher percentage of failed axles on the bogies at the extremities of the trainset.

The root-cause analysis showed that the combination of input forces and actual design could result in a severe fretting phenomenon leading to contact wear. The acceptance criterion needs to be refined to evaluate the right combination to obtain a sustainable solution:

- By reducing forces induced by the wheel/rail contact (nominal profile, maintenance criteria...); and/or
- By potentially optimizing the design of the axle

On track test results also showed an improvement of track conditions in terms of vibrations level (mainly related to rail corrugation in curves) when compared to January 2021 results where the track was generating a high level of vibration on the bogie. It is logical to consider that these levels could contribute to increase the loads on the assembly during this period of time even if the 2022 tests were not able to provide us with a direct correlation. Some of the axles being recently detected with a clearance could have been affected by a fretting initiation phenomenon in a past period.

### **4.2 Recommendations**

The test results point out that maintenance and operation conditions are key to lowering the stress and the demands on the axle during service.

Given that the track and train design (axle) are "fixed" in the short-term, actions to lower the transversal load could start with any or all of the following:

- Optimizing the wheel profile to adapt to current rail/track geometry
- Improve the friction in curve by greasing the rail gage face
- Find the best compromise in operation profile to lower the curving speed in the most critical curves
- Review the maintenance criteria of track/wheel to avoid prolonged exposure to corrugation

Longer term levers will continue to be investigated in parallel to evaluate and confirm their criticality in the fretting wear occurrence. The long-term levers would not be a replacement for the short-term actions noted above.

- Characterize properly the installed superelevation to check if it is consistent with the speed profile
- Optimize the axle hub to increase locally the margin against fretting
- Optimize the axle design to increase globally the margin against fretting

In the meantime, the current applied fleet control should continue until achievement of an acceptable level of forces/design combination.





## SECTION 5 REFERENCES

[P1]	ADD0000939383	Instrumented Axle Hub Track Test Outline
[P2]	EN13979-1	European standard for technical approval of monobloc wheels
[P3]	IEC61373-3	Railway applications – Rolling stock equipment – Shock and vibration tests
[P4]	OTT-ENG-REP-139_139	Preliminary derailment report for TS19
[P5]	Confederation Line - Pre-Grind Inspection Optical Measurements - Advanced Rail Management (Canada) Inc.	
[P6]	RES-TW-0-GLO1-DCI-0001_(A)	Design Criteria – Alignment and Geometric Design
[P7]	ADD0000938674_rev H	INTERFACE SPECIFICATION

## SECTION 6 List of Contributors

Version	Date	Content of Modification	Author(s)
A	2022-05-09	First issue.	<b>D. SONG</b> Project Engineering Manager CDS Bogie / Le Creusot <b>P. BOICHOT</b> Master Expert, Bogie & Track testing CDS Bogie / Le Creusot <b>C. BENAIS</b> Senior Expert, Bearing & Transmission CDS Bogie / Le Creusot <b>N. SEMBEYEV</b> Design Engineer CDS Bogie / Le Creusot <b>JP. LEFEBVRE</b> Expert, FE Analysis CDS Bogie / Le Creusot

UNCONTROLLED WHEN PRINTED – Not to be used before verification of applicable version number

**"CONFIDENTIAL -TRADE SECRET" - © ALSTOM SA 2020. All rights reserved. Reproduction, use or disclosure to third parties, without express written authorisation, is strictly prohibited.**